QATAR UNIVERSITY

COLLEGE OF PHARMACY

SURFACE COATING OF CARBON NANOFIBER BY MESOPOROUS SILICA: A PROMISING STRATEGY TO REDUCE ITS TOXICITY DURING EMBRYOGENESIS

BY

GHADA AHMED GALAL

A Thesis Submitted to

the College of Pharmacy

in Partial Fulfillment of the Requirements for the Degree of

Masters of Science in Pharmacy

January 2021

COMMITTEE PAGE

The members of the Committee approve the Thesis of
Ghada Ahmed Galal defended on 09/12/2020.

_____
Dr. Ashraf Khalil, PhD
Thesis/Dissertation Supervisor

_____
Dr. Ahmed Elzatahry, PhD
Thesis Co-Supervisor

_____
Dr. Ala-Eddin Al Mustafa, PhD
Thesis Co-Supervisor

Approved:

_____
Mohammad Diab, Dean, College of Pharmacy

ABSTRACT

ABDO, GHADA, G., Masters : January : 2021, Medicinal Chemistry

Title: Surface Coating of Carbon Nanofiber by Mesoporous Silica: a Promising Strategy to Reduce its Toxicity during Embryogenesis

Supervisor of Thesis: Ashraf, A., Khalil.

Although carbon nanofibers (CNFs) have been implicated in biomedical applications, they are still considered as a potential hazard. Conversely, mesoporous silica nanoparticles are generally considered as a suitable and biocompatible material for *in-vivo* use. In this study, we sought to discover a novel strategy leads as a potential approach to overcome CNFs toxicity. We fabricated conventional CNFs and novel CNFs coated with a mesoporous silica layer (MCNFs). They were synthesized by preparing polyacrylonitrile fibers via electrospinning, followed by carbonization at 800 C^{o} in an inert atmosphere. A soft templating strategy was applied to coat CNFs with a mesoporous silica layer. The obtained nanofibers were then characterized by various analytical techniques.

Subsequently, we used avian embryos at 3 days and its chorioallantoic membrane (CAM) at 6 days of incubation to evaluate the impact of synthesized CNFs and MCNFs on the early stage of embryogenesis and angiogenesis. We confirmed our embryogenesis data using *Drosophila melanogaster*. Furthermore, we analyzed the outcome of the effect of CNFs and MCNFs on normal embryonic fibroblast cells. Our data show that mesoporous coating of CNFs resulted in significantly reducing both, embryotoxicity and angiogenesis of the CAM. Additionally**,** we elucidate key regulator genes of embryotoxicity induced by CNFs and MCNFs; thus, RT-PCR analysis was

performed on seven key controller genes; we found that MCNFs did not significantly deregulate expression of the controller genes involved in proliferation, survival, angiogenesis, and apoptosis as compared to CNFs. Consistently, MCNFs significantly have a higher survival probability on D. *melanogaster* compared to CNFs, $P<0.0001$.

In vitro, CNFs & MCNFs cause antiproliferation of embryonic fibroblasts cells (EFCs) with IC50 (70.2 and 79.5 μg/ml, respectively). Concerning cell cycle, only CNFs had significantly arrested EFCs in sub G0 and G2/M phases (17.1± 0.70% and 22.75± 1.76%, respectively). Interestingly, MCNFs downregulated expression of ERK1/ERK2, p-ERK1/ERK2, JNK1/JNK2/JNK3, Bax, and upregulated expression of the anti-apoptotic marker Bcl-2, thus indicating a protective role of MCNFs against apoptosis. Overall, coating CNFs surface with mesoporous silica was found to be an effective strategy to alleviate the CNFs toxicity and potentially more biocompatible for biomedical applications.

Keywords: Carbon nanofibers; Mesoporous silica nanoparticles; Avian embryo; Angiogenesis; Chorioallantoic membrane; Toxicity; Apoptosis

DEDICATION

This Thesis is dedicated to my beloved Dad (Dr. Ahmed) and Mom (Dr. Nada) for their endless love and support throughout my life, my dearest husband (Dr. Hassan) for his understanding, patience, and for constantly being by my side, and finally to my lovely daughter Maleeka.

ACKNOWLEDGMENTS

Foremost, I would like to express my sincere gratitude and appreciation to my mentor, Dr. Ashraf Khalil, for his continuous efforts, motivation, support, and encouragement. And to my co-supervisors, Dr. Ahmed Elzatahry thank you for your endless guidance, continuous support, enthusiasm, and especially for your confidence in me, and Dr. Ala-Eddin Al Mustafa thank you for your assistance, insightful comments, immense knowledge, and motivation. I am very lucky to work with such great scientists, I have acquired a lot of valuable knowledge and skills from them, without you this project would not have been done to this level.

Also, I must express my deepest thanks to Mustafa Zagho (Southern Mississippi) for guiding me in the preparation of carbon nanofiber and mesoporous materials used in this thesis. Also, I would like to thank Abdullah Alashraf Abul Baker (Centre of advanced materials), Mr.Essam Shabaan Attia (Central Lab Unit), and Dr.Mohammed Yousuf (Central Lab Unit) for helping me in the characterization of the fabricated nanocarriers. And Dr. Farhan Cyprian for assisting me in the cell cycle.

Thanks to my friends, colleagues at the MSc program and for their support. I want to express my deep appreciation to my lab colleagues Hadeel as well as Ola, and Shireen for helping me and deep thanks to my lovely friend Munia who has always been by my side. I would like to pay deep appreciation to Dr. Mohammed Izham head of the MSCs program, College of Pharmacy faculty members who have taught me during my study at the MSc programs, and to the administrative staff and dean, Dr. Mohammed Diab, for their continuous assistance and help.

Table of Contents

LIST OF TABLES

LIST OF FIGURES

LIST OF ABBREVIATIONS

ANOVA: Analysis of variance

ATF3: Activating transcription factor-3

BAX: Bcl2 Associated X

Bcl2: B-cell lymphoma 2

CAM: Chorioallantoic membrane

CVD: Chemical vapour deposition

CNFs: Carbon nanofibers

CNMs: Carbon nanomaterials

CNTs: Carbon nanotubes

D. melanogaster: *Drosophila melanogaster*

EDX: Energy dispersive x-ray

EFCs: Embryonic fibroblast cells

ERK: Extracellular signal-regulated kinase

FBS: Fetal serum bovine

FSC: Forward scatter

FOXA2: Forkhead box-A2

GAPDH: Glyceraldehyde 3-phosphate dehydrogenase

IC50: The concentration that gives a half-maximal response

INHBA: Inhibin beta-A

JNK: c-Jun N-terminal kinases

MAPK: Mitogen-activated protein kinase

MAPRE2: Microtubule-associated protein RP/EB family member-2

MCNFs: Mesoporous carbon nanofibers

MSNs: Mesoporous silica nanoparticles

PAN: Polyacrylonitrile

PBS: Phosphate buffered saline

RIPK1: receptor-interacting serine-threonine kinase-1

ROS: Reactive oxygen species

SDS-PAGE: Sodium dodecyl sulfate-polyacrylamide gel electrophoresis

SEM: Scanning electron microscope

SERPINA-4: Serpin peptidase inhibitor-4

SPSS: Statistical Package for Social Sciences

SSC: side scatter

TEM: Transmission electron microscope

TEOS: Triethyl orthosilicate

THF: Tetrahydrofuran

VEGF-C: Vascular endothelial growth factor-C

VGCFs: Vapor grown carbon fibers

XRD: X-ray diffraction

CHAPTER 1: INTRODUCTION

1.1.Carbon Nanomaterials

Limited control over the traditional biomaterials hinders their utilization in the biomedical applications. To tackle this problem, researchers focus has been directed to novel materials that exhibit various, interesting physicochemical properties and improved functionalities (1). Accordingly, carbon nanomaterials (CNMs) have shown several unexpected properties that result in an impressive and promising impact with respect to both scientific and technological output. CNMs dimension varies from 1 nm to 1 μm, which is equivalent to the protein (1-100 nm) and DNA (2-3 nm) size, ion passages size (biological barrier) in vivo in addition to the high tendency to be cleared efficiently and intact via globular filtration (2).

Carbon-based nanomaterials (CNMs) have gained tremendous attention owing to their unique properties in diverse applications stretching from thin-film transistor**,** supercapacitor, biosensing, bioimaging, drug delivery, diagnosis, transparent conducting electrodes, cancer therapy, and tissue engineering (3–9). From the zero-dimension carbon nanodiamonds, fullerene, and dots to the one-dimensional carbon nanofibers (CNFs), carbon nanotubes (CNTs), to the two-dimensional graphene atomic sheets, CNMs have demonstrated a highly efficient class of nanomaterials. Owing to the existence of carbon in various allotropes and nanostructures due to variation in *sp*, sp^2, and sp^3 hybridizations (10,11)

It is established that sp^2 hybridization mediates the distinctive hexagonal lattice of many CNMs, where carbon atoms are attached via two single bonds and a double bond and organized in a trigonal pattern. On the other hand, carbon atoms are linked

by single bonds in a tetrahedral sequence in the cubic crystal diamonds owed to sp^3 hybridization (11). Other carbon structures are obtained by sp^3 to sp^2 carbons transition and it includes octahedral and spherical structures. The formation of closed, zero-dimensional CNMs fullerene (12) or one-dimensional CNMs (carbon nanofiber/ nanotube) (13) or flat, two-dimensional CNMs, (graphene) (14) depending on $sp/sp^2/sp^3$ hybridization ratio. Furthermore, the chemical, magnetic, electrical conductivity, and structural strength characteristics of CNMs are controlled by this ratio (15).

Since CNFs discovery, it has gained a lot of attention as a versatile nanomaterial without apparently limitless applications (13). Interestingly, the investigation of CNFs in the biomedical field has demonstrated an immense and flexible potential through an enormous amount of diverse field, especially in the area of tissue engineering and biosensors. CNFs have been used as a perfect electromechanical actuator for artificial muscles due to their electrical properties (16). Additionally, they have been exploited to detect various biomolecules as a novel electronic. Further investigations have demonstrated that CNFs are fitting scaffolding biomaterials, that has displayed great potential to support and stimulate the growth development of osteoblasts, fibroblast cells, and even neurons (17).

Although CNFs were discovered a few years earlier than CNTs, they have received less research attention than CNTs. Since, both single-walled carbon nanotubes and multiwalled carbon nanotubes are synthesized via discharge and laser ablation. Therefore, their mechanical properties are superior compared to CNFs. Additionally, CNTs exhibit a lower diameter and density than CNFs. Nevertheless, CNFs are considered a perfect alternative for CNTs due to its lower price and economic viability

in several applications. They are also used in combination with CNTs to form bi-filler composites that have synergistic properties (18). Interestingly, CNFs have the highest specific surface compared to all other CNMs and availability to be scaled up easily, which makes it a promising candidate for biomedical applications (19,20).

1.2. Carbon Nanofibers (CNFs)

Carbon fibers (CFs) were synthesized for the first time by carbonizing bamboo and cotton. In 1879, Thomas Edison used the CFs as a filament of a light bulb (21). The first trial by Thomas Edison to fabricate carbon fibers was achieved via dissolving cellulosic substances followed by an extrusion process to obtain the fibers and then carbonization in the absence of air. Then, Hughes and Chambers patented the synthesis of carbon filaments (22). The current fabrication of CFs includes three precursors, petroleum pitch, polyacrylonitrile (PAN), and rayon (regenerated cellulosic fibers). CFs were enormously emerged and developed in several scientific investigations and practical applications (23). CFs are fibrous carbon material with a graphite crystal structure containing a minimum of 92 wt % of carbon atoms (24). CFs are highly anisotropic owing to their graphitic structure along with strong crystalline covalent bonds. CFs were used in stimulating wound healing and designing active scaffolds to stimulate ligament repair. Unfortunately, they led to debris formation due to the induced shear stress resulting from poor forces between graphitic planes. Recently, most scaffolds developed for cartilage repair were unsuccessful due to poor mechanical properties and structural flexibility (25). Thus, improving and optimizing the mechanical properties become the most required goals. The reinforcing capacity of fibers can be enhanced by reducing the diameter; consequently, CNFs exhibit more outstanding reinforcing capabilities than CFs (microfiber) (26). Moreover, reducing the

CFs diameter produces CNFs with a lower number of defects, greater flexibility, higher surface area/volume ratio, better mechanical properties, and increased ultimate tensile strength.

Carbon nanofibers are carbon nanomaterials with a diameter of more than 100 nm. CNFs are considered one of the most crucial CFs family members due to their promising applications in various fields, including self-sensing devices, energy storage, biosensing, reinforcement of composites, and biomedical applications (27,28). Carbon nanofibers are sp^2-based one-dimensional filaments with high surface area, mechanical properties, and flexibility. Nevertheless, they are different in their small diameter from the conventional carbon fibers and vapor grown carbon fibers (VGCFs) (29). They were fabricated for the first time with high performance in the 1950s by Roger Bacon. Later, in the 1960s, CNFs were fabricated from PAN by Akio Shindo via electrospinning followed by carbonization (22). CFs and VGCFs have numerous micrometer-sized diameters. Besides the dimensions, the structure of CNFs is quietly different from CFs. The typical CFs are synthesized from high strength PAN or mesophase pitch with varied preparation conditions such as starting material, heating temperature, and oxidation condition. Unlike CFs, CNFs are mainly fabricated by two approaches; catalytically vapor deposition growth and electrospinning.

1.2.1. Synthesis of Carbon Nanofibers

Two concepts are mainly used to prepare CNFs; catalytically chemical vapor deposition growth and electrospinning.

1.2.1.1. Chemical Vapor Deposition (CVD)

There are two types of CNFs synthesized by catalytic thermal chemical vapor deposition (CVD), the platelet CNFs and the cup-stacked CNFs. Ge and Sattler

discovered the cup stacked CNFs (30). In this approach, various types of metals or alloys are used as the catalyst (such as iron, nickel, cobalt, vanadium, or chromium), capable of dissolving the carbon to form metal carbide. Also, carbon monoxide, methane, syngas (H_2/CO), and ethene serve as a carbon source in the temperature range of 700-1200 K (31). In general, CNFs structure can be controlled by the shape of the catalytic nanosized metal particles. Deposition of the dissolved hydrocarbons as graphitic carbon occurs on the metal surface (32). Figure 1 demonstrates the typical growth approach of the cup-stacked CNFs (33).

1.2.1.2. Electrospinning

Electrospinning is a commonly used approach for the synthesis of CNFs (34). In fabricating CNFs by electrospinning, the polymer nanofiber is used as a precursor for the final CNFs structure. The electrospinning processing parameters determine the characteristics of CNFs. Both PAN and pitches are commonly used in CNFs preparation. Besides, polyimides, polyvinylidene fluoride, polyvinyl alcohol, polybenzimidazole, lignin, and phenolic resins are used (35). Electrospinning is considered as a perfect technique employed to fabricate CNFs and CNFs-based composites. Owing to the uniform dispersion of CNFs in the matrix, the final composites display superior electrical conductivity and highly porous structure (36).

In this concept, the polymer solution is placed in a syringe with a thin-diameter needle (37,38). Afterward, the needle is settled on the holder where a high voltage is applied. This strategy results in the development and accumulation of the fibers caused by the high surface tension. Then, the polymer fibers will be stabilized in the air at 250-300 °C. Subsequently, the nanofibers will be carbonized at elevated temperatures up to 1000 °C under an inert gas atmosphere. The cyano groups in PAN will be cyclized

when exposed to heat at 200-300 ℃ in the presence of oxygen, as shown in Figure 2 (39). Upon further heating in the range of 600-1300 ℃ under an inert atmosphere, the adjacent chains will be fused, producing a ribbon-like ring containing nitrogen atoms at their margins. During the carbonization process, more ribbons will be formed, while more nitrogen atoms will be expelled. Eventually, pure carbon material of graphite structure is formed at the end of this process. This process controls the morphology, purity, crystallinity, and diameter of CNFs. Furthermore, the carbonization process changes the weight and volume and reduces CNFs diameter (39).

1.3. Biomedical Applications of Carbon Nanofibers

CNFs are mainly explored as electrodes in batteries and supercapacitors due to their excellent electrical conductivity properties (35). Surprisingly, CNFs demonstrate a promising potential candidate for biomedical applications due to their excellent mechanical, structural, and electrical properties. Interestingly, CNFs are advantageous over CNMs because of their excellent structural resilience and versatile fabrication procedures (electrospinning followed by carbonization). Additionally, they have much greater hollow interior diameters ranging from 5 nm to 400 nm, which is favored in a wide range of biomedical applications (35). In this section, recent biomedical applications mediated by CNFs are reviewed, Figure 1.1.

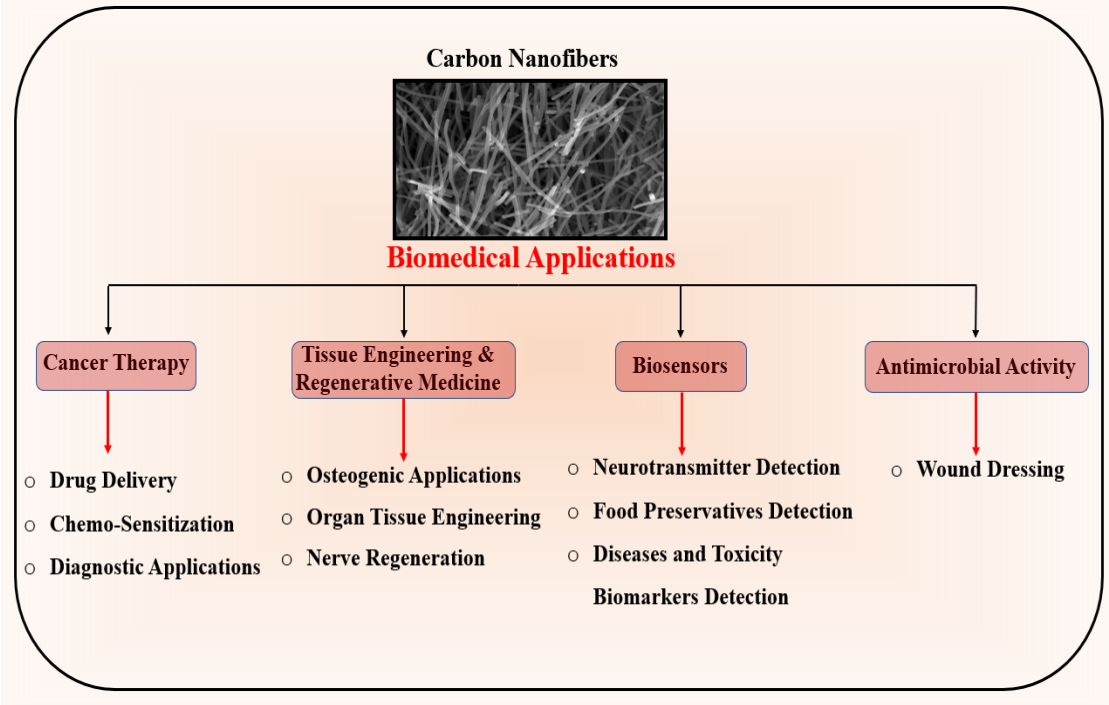

Figure 1. A Summary of the recent contribution of carbon nanofibers in biomedical applications

1.3.1. Cancer Therapy

The most applicable treatment types to expand the lifespan and survival rate of cancer patients are surgical tumor removal and chemotherapeutic implementation. Interestingly, contributing CNFs in cancer therapies has enhanced both diagnosis and therapy schemes' performance and effectiveness. CNFs showed a promising strategy to overcome chemoresistance by improving prostate and bladder cancer cells' sensitization to chemotherapeutics.

Kati et al. (40) reported the increased chemo-sensitization of prostate cancer cells (PCa) to traditional chemotherapeutics (docetaxel and mitomycin C) using CNFs and CNTs. CNFs incorporation decreased PCa cells' viability to less than 70% without using high amounts of mitomycin C and docetaxel approximately (7- and 17- fold, respectively). Moreover, CNFs displayed a long-term inhibition of proliferation and

superior impact on cellular function over CNTs. Dilip et al. (41) developed zinc oxide nanoparticles attached to graphitic CNFs by a simple co-precipitation method. These novel composites resulted in improving growth inhibition and potent synergistic toxicity against Hela cells. In another study, Chih et al. (42) fabricated hydrophilic CNFs via hydrogenation of CO_2 on $NiNa/Al_2O_3$. This composite was designed for the targeted delivery of doxorubicin (DOX). DOX loaded CNFs efficiently targeted and killed Hela cancer cells with minimal toxicity toward normal human primary fibroblast cells. A successful attempt was released to investigate the delivery of carboplatin *in vitro* using CNFs and CNTs as nanocarriers, and the results confirmed their biocompatibility with no significant toxicity (43). The release pattern of carboplatin from CNFs and CNTs displayed a marginal and constant release, respectively. Carboplatin loaded CNTs were more toxic to cancer cells than CNFs (43). However, these results were inconsistent with those reported by Jessica et al. (44). In this study, the effect on cellular uptake, function, and capability to improve the cancer cell sensitization, compared with the traditional chemotherapeutics carboplatin and cisplatin, was discussed using CNFs MWCNTs. Both CNMs (1-200 μg; loading) demonstrated a low to moderate cellular activity alteration, where CNFs were more destructive than CNTs. Moreover, the cancer cells were efficiently internalized with CNFs, and the cellular accumulation of carboplatin was improved 28% by CNFs, compared with using carboplatin without CNFs incorporation (44). Interestingly, In 2020, Jiamu et al. introduced a novel smart nanocarrier system based on porous CNFs (45). This nano-vehicle overcome the hydrophobicity debate of CNFs via layer by layer treatment and common acid modification of CNFs surface. These vehicles offered a superior dispersibility, photothermal conversion ability, near-infrared absorbance, and

drug delivery dual responsive. Doxorubicin loaded porous CNFs exerted a significant tumor inhibition efficiency in *vitro* and *in vivo* without any side effects.

1.3.2. CNFs-Based Biosensors

Due to their high aspect ratio that causes enhanced electrical conductivity, low cost, and biocompatibility, CNFs represented a promising nanoprobes generation. Their stacked-cup morphology results in generating exposed reactive edges plane that increases the electron-transfer rate and renders them exceptionally for biosensing applications (46). Table 1 summarizes the analytical characteristics of CNFs-based biosensors.

1.3.2.1 Neurotransmitter Detection

CNFs were employed in electrodes fabrication for neurological applications to detect electroactive neurotransmitters (47). CNFs were aligned within polyethylene (CPE) sheets composites *in situ* during thermal drawing. A steady electrical recording process characterizes the designed neural probe. The composites displayed higher biocompatibility than chronic implantation for neuroscience applications. Besides, these CNFs-based neural probes are biocompatible with surrounding brain tissues with minimal triggered foreign body responses, highlighting additional advantages over conventional materials. Recently, Hong et al. synthesized molybdenum disulfide nanosheets arrays (of Golf balls shape) deposited on CNFs to efficiently detect dopamine (48).

1.3.2.2. Food Preservatives Detection

Bisphenol A is widely used in food packaging applications. It has an endocrine-disrupting effect as its structure mimics the estrogen hormone. Sung et al. introduced a field-effect transistor sensor based on aptamer established on multichannel CNFs (49).

These sensors were formed by oxidation of multichannel CNFs by HNO_3 and H_2SO_4 solutions to form a carboxyl group on the CNFs surface, followed by immobilization on an amine-functionalized electrode. The resulting sensors have excellent sensitivity and selectivity compared with bisphenol at a relatively small concentration of 1 fM. Phosphorous doped CNFs prepared by CVD with excellent pressure annealing formed a 3D great hierarchical helical structure exhibiting rapid electron transfer. This composite demonstrated high electrocatalytic activity and sensitivity to detect carbendazim in food sample food (50).

1.3.2.3. Diseases and Toxicity Biomarkers Detection

Through immobilization of an aptamer or antibody on VACNFs, the antibody or aptamer's conjugation and the ricin are characterized and detected efficiently by electrochemical impedance spectroscopy (51). Periyakaruppan et al. designed label-free CNFs NEAs to detect the cardiac troponin-I biomarker in the early examination of myocardial infarction (52). Moreover, VACNFs nanoelectrodes were prepared via plasma improved CVD to detect c-reactive proteins (cardiac disease biomarker) (53).

Phenolic compounds are hazardous substances that could lead to cancer infection and loss of immunity. Ni and Cu alloy nanoparticles loaded CNFs mixed with laccase and Nafion showed a promising detection and sensitivity towards hydroquinone (54).

Table 1. Summary of the analytical characteristics of biosensors based on CNFs.

Analyte Detected	Sensing Materials	Fabrication Mechanism	Applied Potential	Sensitivity	Linear Range	Detection Limit	Highlights	Ref.
Dopamine (DA)	Arrays of MoS_2 nanosheets deposited on CNFs	Electrospinning preparation of CNFs followed by *in situ* growth of MoS_2 on its surface	+0.17 V	6.24 $\mu A \cdot mM^{-1} \cdot cm^{-2}$	1–60 µM	36 nM	-Detection was done without the interference of uric acid -MoS_2 nanoparticles shape resemble golf ball (2 µM)	(48)
Dopamine (DA) & Serotonin (5-HT)	Arrays of vertically aligned carbon nanofibers	Plasma enhanced chemical vapor deposition	5 Mv	N/A	1 µM to 10 µM & 100 nM to 500 nM	50 nM for dopamine & 250 nM For serotonin	-Ability to discriminate between DA, 5-HT and AA	(55)
Dopamine	Fc labeled tetrapeptides attached to (NEAs) fabricated with VACNFs	CNFs are directly grown on top of (ta-C)	-100 mV	N/A	N/A	1 µM	-Detection of DA in the presence of AA -Ta-C +CNF detect nonenzymatic of glutamate at physiological pH	(56)
Bisphenol A	FET sensor using aptamer modified multichannel CNFs	Electrospinning preparation of CNFs followed by thermal treatment. Then, acid treatment to immobilize the aptamer	50 mV	N/A	$10^0 - 10^4$ fM	1 fM	FET sensors could be reused over 4 weeks	(49)
Carbendazim	Phosphorus-doped helical carbon nanofibers	Chemical vapor deposition with high-pressure annealing	0.6 to 1.2 V	0.92 A $mol^{-1}L$	0.1 to 35 µmol L-1	0.038 µmol L^{-1}	Determination of carbendazim in food samples	(50)
Ricin	Antibody and aptamer probes immobilized on a NEAs consisting of VACNFs	Plasma-enhanced chemical vapor deposition	−0.4 and 0.8V	N/A	N/A	5 µL of 0.5 µg/mL	This prob could be regenerated multiple times to create a reusable biosensor	(51)
Cardiac troponin-I	VACNFs	Plasma-enhanced chemical vapor deposition a silicon wafer	−0.4 and 0.8 V	N/A	0.25−1.0 and 5.0−100 ng/mL with r= 0.94528	~0.2 ng/mL	-An inexpensive, easy, and label-free electrochemical	(52)

Analyte Detected	Sensing Materials	Fabrication Mechanism	Applied Potential	Sensitivity	Linear Range	Detection Limit	Highlights	Ref.
					and 0.89790, respectively		impedance spectroscopy-based biosensor - Detection limit 25 times lower than ELISA at 5 ng/mL	
C-reactive protein	VACNFs	Plasma-enhanced chemical vapor deposition	-400 mV to 800 mV	N/A	N/A	11 ng/ml	Clinical relevance of the detection limit value	(53)
Spinal muscular atrophy protein	CNFs Electrode immobilized with SMN antibody	The Immobilization achieved via Electroreduction of diazonium salt	0.3 to -0.4 V	N/A	1.0 pg ml^{-1} to 100 ng mL^{-1}	0.75 pg/ml	CNFs immunosensor was the most responsive platform among other carbon-based immunosensor	(57)
Hydroquinone	Nickel and copper alloy nanoparticles loaded on CNFs	1)Electrospinning followed by carbonization method. 2)NiCu CNFs were mixed with Lac and Nafion.	-0.8 to 1.2 v	1.5 µA $µM^{-1}$	4×10^{-7} –2.37×10^{-6} M	90 nM	This biosensor was capable to detect hydroquinone in lake water	(54)
Hydroquinone, catechol and resorcinol	Cobalt-iron selenides embedded in porous carbon nanofibers	Electrospinning followed by carbonization	N/A	N/A	0.5-200, 0.5-190- and 5-350-mM for HQ, CC and RS, respectively	0.13, 0.15 and 1.36 mM for HQ, CC and RS, respectively	This biosensor could be extrapolated to detect HQ, CC and Rs in actual samples	(58)
Glucose	Cu(I)–C18 complex–CNF paste electrode	A randomized copper oxides microelectrodes array was dispersed within CNF paste	−0.5 to +1.5 V	5419.77 $µA \cdot mM^{-1} \cdot cm^{-2}$	0.02–0.14 mM	0.048/0.07 µM	-	(59)
Glucose Oxidase	Nitrogen-doped carbon nanospheres@carbon nanofibers	Electrospinning of polypyrrole nanospheres doped polyacrylonitrile nanofibers followed by thermal treatment	-0.40V	13.5 $µA \cdot mM^{-1} \cdot cm^{-2}$	12–1000µM	2µM	-	(60)

Analyte Detected	Sensing Materials	Fabrication Mechanism	Applied Potential	Sensitivity	Linear Range	Detection Limit	Highlights	Ref.
Cortisol	Nitrogen-doped multidimensional CNFs	CNFs were functionalized by thermal, and acid treatments followed by antibody attachment	–0.5 V to + 0.5 V	N/A	100 aM to 10 nM	100 aM	-	(61)

1.3.3. Tissue Engineering and Regenerative Medicine

Among the reinforcing materials, CNFs are considered a cheaper and safer alternative among CMNs (62). Other features of CNFs are their functionalization flexibility and ease of dispersion compared to CNTs. Furthermore, CNFs improve structural stability, mechanical strength, and conductivity of the matrix. Thus, they fasten the fractured bone's healing process by providing appropriate piezoelectric properties and acting as nano-vehicles for sustained drug delivery. Besides, they are flexible for uniaxial orientation and less probably to curve in matrices (62). The fiber’s size is closely similar to hydroxyapatite crystal and fibrillar proteins, such as integrin proteins and type 1 collagen. Therefore, CNFs are considered as promising materials in bone-implant applications.

1.3.3.1. Osteogenic Applications

Generally, CNFs composites for bone repairing are prepared by functionalizing the CNFs surface with surfactants, acids, and oxidants to provide ketonic, carboxylic, and hydroxyl groups. As a result, properties, dispersion, compatibility, and interactions of CNFs with hydroxyapatite (HAP) matrix, are markedly improved (63). Potential nanofibrous scaffolds can be designed by incorporating CNFs into polycaprolactone/mineralized HAP (64). These composites noticeably improved both elastic modulus and adhesion properties. Besides, human osteosarcoma's cell viability was substantially improved for CNFs-containing composites compared to those without CNFs. *In vivo* studies revealed soft fibrous tissue growth with no significant inflammatory response.

CNFs demonstrated great potentials in neural tissue regeneration applications. For instance, CNFs neural ships were introduced for dual monitoring of neurochemical

and neuroelectric activity (65). Akira and co-workers patented nerve scaffolds designed with internal CNFs yarn (17). The yarns supported the nerve fibers and provided additional surfaces for nerve fibers growth without triggering undesirable events, such as nerve pain and weakening nerve function. Esmaeil et al. cultured human endometrial stem cells on aligned and random CNFs (66). Both CNFs prompted the proliferation and differentiation of neural cells.

1.3.3.2. Organ Tissue Engineering

The cumulative incidence rate of bladder cancer recurrence at 5 years is 31-78% (67). To improve bladder reconstruction and resection processes, it is essential to replace bladder tissues, which can alleviate the risk of cancer relapse and metastasis. CNFs were employed to fortify polyurethane for a developed prosthetic that promotes the normal primary bladder's regeneration and function with reduced threat of cancer recurrence (68). Interestingly, CNFs were also used to reinforce poly-ε-caprolactone (PCL) scaffolds for meniscal tissue engineering (69). Compared to pristine PCL, the composite scaffolds exhibited better cytocompatibility, higher mechanical and electrical properties, and promoted cell proliferation. Both rosette nanotubes (RNTs) and CNFs were incorporated by Meng et al. into poly(2-hydroxyethyl methacrylate) hydrogel offering the support needed for cardiomyocyte (70).

1.3.4. Antimicrobial Activity Applications

CNMs exhibit excellent bactericidal and biocompatibility properties (71). Generally, the bactericidal activity of CNMs results from both physical and chemical activity. Physically, CNMs cause reasonable structural destruction of microorganism’s cell walls and mitochondria, including DNA mutations. Furthermore, CNMs

chemically interact with microorganisms surface resulting in electron drainage from the external microbial surface and producing toxic chemicals such as reactive oxygen species (ROS), leading to oxidative stress on microorganisms' cells (72).

CNFs offer excellent thermal and mechanical stability to antibacterial materials. Therefore, researchers paid their attention to design CNFs-supported wound dressings. For instance, composites' antibacterial activity consisting of surfactant-mediated Ag and Cu nanoparticles dispersed in hierarchical carbon ACFs/CNFs was examined against *E. coli* and *S. aureus* (73). The results demonstrated that complete inhibition of bacterial growth was achieved after 72 hours. Additionally, Pratibha et al. (74) designed an efficient wound dressing with rapid healing for diabetic patients. The wound dressing consisted of immobilized yeast extract and dispersed Cu nanoparticles in CNFs. The wound dressing provided significant simultaneous glucose and bacterial infection control.

1.4. CNFs Toxicity and Challenges

Regardless of fruitful outcomes that result from the implementation of CNFs in biomedical applications, potential hazards are still considered. Besides, despite the strong preclinical shreds of evidence of their significant artificial intelligence contributions, they are far away to be approved for adoption in real clinical practices. CNFs showed outstanding and promising contributions in biomedical applications, including tissue engineering and drug delivery. However, limited evidence about CNFs toxicity, cytocompatibility, and dispersibility, are considered primary concerns that hinder them from being used as successful biomaterials or clinically adopted. There are contradictory outcomes of several research studies underlying CNF’s safety (75). To date, it should be pointed out that there are no general guidelines addressing evaluation

procedures of CNFs toxicity, mainly due to a lack of sizeable reference materials. The majority of toxicity studies were devoted to assessing inhalation toxicity (76). Remarkably, tissue engineering results suggest the relatively low toxicity of CNFs (77). It is worth mentioning that there is difficulty in investigating the health effect of CNMs. Numerous factors affect and control CNFs toxicity, including surface area, chemical structure, purity, shape, the tendency to agglomerate, and functionalization (75). Research studies on animals revealed that CNFs exposure led to systemically and locally inflammatory cardiovascular adverse effect diseases and oxidative stresses (78). Few epidemiological studies were conducted on humans; nevertheless, they were limited to exposure evaluation and single workplaces (79). To illustrate, current occupational results are limited because the manufacturing and utilization of CNMs are relatively recent, and the workforce size is small. No reports discuss CNFs release mechanism and physicochemical characteristics of the released material, to the best of our knowledge. Additionally, CNFs concentrations used in toxicity studies are usually expressed in μg/mL, which are significantly larger than the real concentrations used in clinical settings, resulting in unreasonable toxicity values.

Unfortunately, several studies demonstrated the non-functionalized hydrophobic nature of CNFs and heavy metal impurities' presence in more cytotoxic incidences (80). These results conflicted with other studies showing the functionalization of CNMs with carboxyl, carbonyl, or/and hydroxyl groups, inducing higher significant toxicity than unfunctionalized ones (81). Additionally, the physical size (diameter and length) of CNFs have also contributed to more cytotoxicity than corresponding smaller and thinner forms (82). Recently, eliminating CNFs using post-treatments has attracted the scientist's interest. However, some studies suggested that

functionalized CNTs will be cleared through renal excretion (2). To date, no research reports studied the long or short fate of CNFs after systemic administration. Recent strategies are capable of overcoming some of these concerns. For example, hydrophobicity, poor biocompatibility, large aggregation tendency, and contamination with heavy metals were alleviated using improved purification techniques and chemical surface functionalization (nitrogen doping and acid treatment) (83). To summarize, using different forms with diverse purities, morphologies, concentrations, exposure, and characterization procedures highlight the reason behind the lack of reliable CNFs toxicity results. Thus, there are urgent needs for CNFs toxicity investigations in-depth and protocols with sizeable reference materials, to harmonize research on exposure, safety, occupational health, and administration assessments.

1.5. Future Prospects

CNFs research is dedicated to biomedical applications, including tissue engineering and biosensors. Applying CNFs in other biomedical applications, including gene delivery and bioimaging, is lack in the literature. It is noteworthy to mention that majority of these biomedical applications involved the use of CNTs, graphene, and fullerene while using CNFs in these areas is still rarely cited. Hence, more efforts and attention should be devoted to unveil and explore the potential advantages of implementing CNFs. Finally, the scarcity of validated data on the potential toxicity of CNFs should trigger scientists to complete the dataset needed for CNFs risk assessment. For instance, this task can be accomplished by running short- and long-term chronic animal bioassays and standard tests, to closely simulate real conditions needed for occupational, local, and systemic administration of CNFs.

1.6. Executive Summary

- Throughout this review, carbon nanofibers (CNFs) open up a new era for extraordinary biomedical applications to the next generation.
- CNFs surface functionalization guarantee their biocompatibility, several reported outcomes emphasized CNFs ability to boost the effect and chemosensitization of anticancer drugs for different types of tumors with minimized drug side effects.
- CNFs coupling with metallic nanoparticles or organic substances CNFs can be employed as efficient and unique biocompatible reinforce materials, biosensors, perfect platforms to support nanoparticles and immobilize biomolecules, and wound dressing supports.
- Implementing CNFs remarkably developed artificial joints and supported the regeneration and growth of tissues, organs, and nerves.
- To date, there are no general guidelines for the evaluation of CNFs potential toxicity due to lack of sizeable reference material. Thus, there are urgent needs for CNFs toxicity deep studies with sizeable reference materials, to harmonize research on exposure, safety, occupational health, and administration assessments.

2. Mesoporous Silica Nanoparticles

Among widely known nanostructured materials, mesoporous silica nanoparticles (MSNs) are extensively employed as nano-carriers for drug delivery applications. MSNs can be functionalized-designed by various synthetic methods. Their morphological properties determine the type of application of these materials. International union of pure and applied chemistry (IUPAC) define the mesoporous materials as those with pore size ranging between 2 and 50 nm arranged in an organized pattern. Mesoporous silica nanoparticles (MSNs) have exceptional properties such as specific surface area, large pore volume, and good chemical and thermal stability (84–86). It was Mobil Corporation laboratories who first introduced MSNs in 1992 (87). Afterwards, in 2001, Regi et al. reported the fabrication of MCM-41 mesoporous silica as a drug nano cargo for the first time. Since then, research is focused on mesoporous silica nanocarriers. The common synthesis methods of mesoporous silica are either based on evaporation-induced self-assembly or the SOL-GEL process (87–89). The widely known types of MSNs are MCM-48 as well as MCM-41 and were proposed as catalysts. Extensive studies were done on these materials in attempt to fine-tune the structure of the product materials with respect to pore size. MCM-41 has been widely investigated as a promising potential candidate for drug delivery applications (90,91). Another class of MSNs widely employed for biomedical purposes was fabricated by a team of researchers at the University of California, Santa Barbara, known as SBA (92). As compared to other MCM- nanomaterials, SBA silica mesoporous nanomaterials is distinguished by the relative larger pores.

2.1 Toxicity of Mesoporous silica nanoparticles

A few studies have reported the toxic effects of silica nanoparticles in human cells due to their ability to generate reactive oxygen species (ROS) that result in apoptosis (93–96). However, on the contrary, investigations showed that MSNs are not toxic; this contrary data is dependent on several parameters such as Z-potential, size, shape, synthetic route that determine the number of silanol on their surface (97,98). It has been stated that MSNs are internalized easily in most normal and tumor cells without causing detrimental impacts on cellular differentiation, proliferation, and growth (32–34). Furthermore, a study analyzed the toxic effect of MSN in both mice as well as embryo models. MSN-exposed mice for 42-days showed no signs of distress (anemia or loss of appetite), thus indicating, that MSN had no adverse effect in mice (99). On the other hand, in embryos, MSN exposure during early gestation led the embryos to be underweight with reduced levels of reactive oxygen/nitrogen species, whereas embryos exposed to MSNs during late gestation had non-significant larger weight in addition to increasing levels in granulocyte-colony stimulating factor. More significantly, an *in-vivo* comparative study between multiwalled carbon nanotubes (MWCNTs) and MSNs administered orally and intraperitoneally to albino mouse showed a significant increase in liver enzymes (aspartate aminotransferase and alkaline phosphatase) along with total protein (TP) levels in the group receiving MWCNTs alone, indicating that MWCNTs are more toxic than MSNs even in smaller doses (100).

3. Oviparous Species

In medical and basic research, animal models play a key role (101). To illustrate, the advances and progress in the area of regenerative medicine, drug discovery and delivery, and cancer research among others are greatly based on *in vivo* studies to confirm the *in vitro* outcomes, as well as establish new therapeutic approaches. Nevertheless, there are considerable ethical, technical, and practical strains regarding the use of conventional rodents and large animals in experimental research (101). Oviparous species provide early access to embryonic stages and the capability to study the maturation of embryo (utero until hatching) (102). Thus, it offers superior knowledge in developmental biology. Among these models are zebrafish, Xenopus, Drosophila, and chick embryo.

3.1. Chicken Embryo

Chick embryo grant a crucial perception and insight into organogenesis as well as development (102)**.** They also exhibit high reproducibility besides they are easy to handle and economical. Avian embryos are widely used to reveal embryonic development mechanisms. Furthermore, they provide the flexibility to analyze and study the expression of desired genes at certain stages of organogenesis (103). This in addition they allow access under a stereomicroscope for injection and manipulation. Succeeded by non-invasive controlling and live imaging *in ovo* throughout subsequent development.

A chicken embryo is also advantageous in investigating and evaluating the toxicity at the whole functioning organism level. Owing to their lack of a blood-brain barrier, rapid growth, capability to isolate them from the external environmental influence, and high sensitivity to external treatments and manipulation, chicken embryo

act as a superior model in toxicity evaluation (104,105). As fast development and growth models they are a suitable candidate for anti- and pro-proliferative mechanisms characterization at the molecular level (106). Besides the profit of chicken embryo in providing insights into the developmental process, they also offer the flexibility to easily ablate the tissues and form tissue grafts in the early stages of chicken embryos (107). It is worth noting that both the National Institute of Health (108), USA, Association of New England Medical Center and the institutional Animal Care and Use Committee (109) authorized the use of chick embryo in experimental studies at any time before they complete the 14^{th} day of their gestation time without ethical imitations or previous protocol consent.

The chick embryo chorioallantoic membrane (CAM) is the external extra-embryonic membrane in which they permit the gaseous exchange and transportation of calcium between the embryo and its atmosphere, due to their high vascularization (110). The CAM provides both practical and technically simple easy approaches to study complex biological models exhibiting well established vascular tissue.

3.1.1. Angiogenesis

It is well established that angiogenesis is a crucial biological process that includes the formation of new capillaries from the pre-existing blood vessels (111). In mammals, angiogenesis occurs during embryo development, pregnancy, wound repair, tissue regeneration, and reproductive cycle (112). Additionally, the formation of new blood vessels supplies the growing cells with oxygen and nutrients needed to rebuild the damaged tissue (113). Angiogenesis is a complex mechanism based on the balance of pro-angiogenic factors as fibroblast growth and vascular endothelial growth factor (VEGF) and anti-angiogenic factors as angiopoietin 2 and angiostatin (111). The basic

fibroblast growth factors is a potent angiogenic molecule, where it is capable to regulate and monitor the functioning and growth of vascular cells such as smooth and endothelial muscle cells, through the stimulation of new blood vessels development and growth (114). On the other hand, VEGF is a well known regulator of angiogenesis, besides it more efficient in stimulation of differentiation of endothelial than basic fibroblast growth factor.

Impairment of the angiogenesis process observed in hypertension, ischemia, respiratory distress, cardiovascular disease as well as neurodegeneration. On contrary, tumor growth, rheumatoid arthritis, atherosclerosis, psoriasis, and asthma are characterized by significantly excessive angiogenesis (115). Interestingly, tumor growth, development, and metastasis are depending mainly on blood vessel formation. Therefore, Suppression of angiogenesis in tumors will subsequently lead to tumor regression and induction of metastasis which is considered the key goal in cancer treatment (116). Anti-angiogenic materials have been widely investigated for anti-cancer therapy (117). VEGF inhibitors are currently approved as an anticancer therapy in a clinical setting. Nevertheless, VEGF inhibitors are efficient only in certain cases and can cause serious toxicity. Thus, optimizing therapeutic agents are mandatory to prevent their adverse effects on healthy cells. Several reports have shown that CNMs are potential promising treatment in cancer through reducing angiogenesis by inhibiting angiogenic signaling pathway and demonstrate low toxicity (112). The antiangiogenic characteristics of CNMs are a double-edged sword. To illustrate, such properties are advantageous for the treatment of disease, while in normal cells, it results in severe defects and embryo lethality due to impairment of vascular system growth and accordingly the oxygen and nutrient supply to normal tissue (118). Moreover,

angiogenesis disruption has been introduced as a sensitive approach for the evaluation of the developmental toxicity of environmental substances (119).

3.2. *Drosophila Melanogaster*

Drosophila melanogaster (*D. melanogaster*) is widely known as the fruit fly and is considered as an excellent model to study various purposed stretching from fundamental genetics to toxicology studies and tissues and organs development (120). In 1990, *D. melanogaster* was first proposed by Thomas Hunt Morgan as a model organism for research (121). Since then, novel discoveries were made through genetic research carried out using D. melanogaster as a genetic model (122). Interestingly, the genome of the Drosophila is 60 % homologous to the human's genome. Furthermore, approximately 75 % of the human genes that cause diseases are believed to have homologs in flies (120). These characteristics, together with a short generation time (lifespan), the presence of strong genetic tool, ease of handling, and low costs of maintenance, enable to investigate complex pathways related to biomedical research (i.e toxicity and cancer). Lately, D. melanogaster was developed as an excellent model for toxicology studies (Drosophotoxicology) (84,123,124). Drosophila model has gained attention in understanding toxicity mediated by nanomaterials. Whereas, it can survive for approximately 40 up to 60 days after eclosion. Therefore, it enables researchers to study efficiently the potential nanotoxicity at different adult flies ages (125). Moreover, chronic nanotoxicity investigations on genome stability, reproduction, and development can be easily carried out due to its relatively short lifespan. *Drosophila* embryonic stage gives the profit to carry out developmental studies to study the effect of nanoparticle exposure on organogenesis, neuronal development, and cell fate determination (126). Besides, adult *Drosophila* is

physiologically comparable to those of humans in terms of the brain, reproductive tract, liver, kidney, and heart. Taking into account theses similarities between *Drosophila* and human, *Drosophila* serves as an excellent model to investigate organ-specific toxicologic studies. (126) In addition, they demonstrate high sensitivity to different chemical composition as well as physical variation (i.e. size, dimensions, coating, and surface area).

It was noticed that different exposure route of carbon nanomaterials provokes a different response in the *Drosophila* model. Recently, *D. melanogaster* was extensively used as a model for nanomaterial toxicity investigation. Single-walled CNTs and carbon black were introduced to *Drosophila* in a dry form via supplying it as a powder to the bottom of closed glass vials without food and water (to correspond human dermal exposure) (127,128). These carbon nanomaterials were found to have the ability to adhere firmly to flies' surface cause loss of locomotor function and their mortality within a couple of hours. Whereas, respiration defects are the prime cause of mortality mediated by these carbon nanostructures in *Drosophila* via partial blockage of spiracle openings. However, multiwalled CNTs failed to induce genotoxicity in *Drosophila* (129). On contrary, incorporation of carbon black, fullerene C60, single-walled or multiwalled CNTs in *Drosophila's* food during their larval stage causes tissue sequestration but no noticeable effect on egg or survival tendency (1mg/g of food) (128). In addition, a recent investigation stated that chronic exposure of *Drosophila Melanogaster* to 100μg/ml of CNFs showed no significant developmental toxicity compared to a higher dose (1000μg/ml); nevertheless, CNFs triggered the activation of the antioxidant defense system due to reactive oxygen species production (130).

4.Thesis Objectives

Despite the great and promising contribution of CNFs to biomedical applications. However, the lack of consistent evidence about their toxicity hinders their clinical application. To date, only a few studies investigated CNFs toxicity, the majority of these investigations involved *in-vitro* models (131,132). Notably, CNFs have demonstrated toxicity in human lung cells through the induction of apoptosis by reactive oxygen species (ROS) production (133,134). Nevertheless, CNFs mediated scaffolds showed no toxicity *in-vivo* (25,64,135,136). On the other hand, several investigations showed that MSNs are not toxic; based on several parameters such as Z-potential, size, shape, synthetic route that determine the number of silanol on the surface (97,98). Mice exposure to MSNs for 42-days has no adverse effect on the behaviors that indicates distress (i.e anemia, loss of appetite..etc.). While the majority of investigations are geared towards adult animals or populations; it is widely known that embryos of various species are more vulnerable to environmental effects and contaminates. Therefore, there is an urgent need for implementing solutions & new strategies to overcome and alleviate the toxicity of CNFs. Thus, Therefore, we speculate that the surface coating of CNFs with mesoporous silica would significantly enhance its biosafety.

Objective 1: To synthesis CNFs and coating it for the first time with a mesoporous silica layer (MCNFs). Then, fully characterize and verify the structure of both fabricated CNFs & MCNFs.

Objective 2: To evaluate and compare the impact of CNFs & MCNFs on the early stage of normal development and angiogenesis using an avian embryo as well as its

CAM as a model.

Objective 3: To study the impact of CNFs & MCNFs on the expression patterns of a set of genes concerned with crucial biological events in the avian embryo.

Objective 4: To investigate and compare the effect of CNFs & MCNFs on cell viability, cell cycle progression, and apoptotic biomarkers using embryonic fibroblast cells.

Objective 5: To confirm the embryogenesis outcome of CNFs and MCNFs by exploring their effect on normal development using another *in-vivo* model (*Drosophila melanogaster).*

CHAPTER2: MATERIALS AND METHODOLOGY

2.1. Materials for the fabrication of CNFs & MCNFs

Polyacrylonitrile (PAN Mw 150,000, Ethanol (FA, 98.0%) was purchased from Aladdin Industrial Inc., China. Poly (propylene oxide)-*b*-poly (ethylene oxide)-*b*-poly (propylene oxide) triblock copolymer Pluronic F127 was supplied by Sigma-Aldrich. Tetrahydrofuran (THF) & Tetraethyl orthosilicate (TEOS) were supplied by Shanghai Chemical Corp. Ethanol (99.7%), Dimethylformeldahyde, NaOH, HCL (supplied by Sigma-Aldrich), and deionized water were used throughout this study.

2.2. Experimental

2.2.1. Fabrication of the carbon nanofibers and mesoporous carbon nanofiber

2.2.1.1. Synthesis of carbon nanofibers:

Carbon nanofibers were prepared using PAN solution (10% PAN/ dimethylformeldahyde (DMF)) by mixing 1 g of PAN with 9 g of DMF in a beaker and stirring overnight. Once the PAN solution was completely dissolved, the solution was placed in a size 9 needle and placed in an electrospinning apparatus, the flowrate of the needle was fixed around 0.3m/ hour. At the tip of the needle, a DC electric charge was placed to allow evaporation of the solution on ejection to create nanofibers, with a foreseen voltage of 8.0 KV. The drum collector was covered with aluminum foil and placed at a distance of 12 cm and spun at 500 RPM. Later, the resulting PAN nanofibers were collected from the collector and placed in a tube furnace (GSL 1500X OTF). The nanofibers were then stabilized by carbonization at 800 ºC in an inert atmosphere (under argon gas flow). The heating process was as follows: gradual heating, from 24ºC to 200ºC for 35 minutes, stabilization process at 200ºC for 120 minutes, then the

temperature was raised from 200ºC to 800ºC during 120 minutes in an inert atmosphere, and then left to guarantee the complete carbonization at 800ºC for 300 minutes, followed by cooling down period.

2.2.1.2. Coating Synthesized carbon nanofiber with a mesoporous silica layer:

To prepare a mesoporous silica solution, 0.1 g Pluronic F-127 was mixed with 5 g tetrahydrofuran (THF) and 0.1 gm 0.1 M hydrochloric acid (HCl) for two hours then, 0.3 g tetraethyl orthosilicate (TEOS) was added and stirred for 30 min. The CNFs were dipped into the mesoporous solution for 5 seconds. The soaked CNFs were placed in a tube furnace and heated from 24 ºC to 350 ºC for 35 min and then baked at 350 ºC for 5 hours under argon flow. The obtained CNFs and MCNFs were sonicated in an organic solvent (ethanol), the solvent was then removed completely via a rotary evaporator. Finally, it was resuspended in deionized sterile for a final concentration of 1mg/1ml water and subjected to ultrasonication for 1 hour to obtain a homogenous suspension.

2.2.1.3. Characterization of carbon nanofibers & Mesoporous carbon nanofibers:

The prepared CNFs & Mesoporous carbon nanofibers (MCNFs) surface morphology was examined using scanning electron microscopy (SEM) equipped with energy dispersive X-ray (EDX). SEM images were captured using FEI NOVA NanoSEM 450. X-ray diffraction was employed to investigate the crystal phase of particles of the as prepared CNFs and MCNFs utilizing PAN analytical X-Ray diffractometer coupled with a Cu-Kα1 as a source of radiation (λ=1.5405Å). The morphology of the as-prepared CNFs and MCNFs was examined using Talos Transmission Electron Microscope (FEI), operated at 200 KV, and provided with a new Ceta 16 M camera. Furthermore, CNFs & MCNFs structure and phase were confirmed

using Thermofisher Scientific (DXR2 Smart) Raman Microscope to obtain the Raman spectra of the samples, at a laser wavelength of 532 nm.

2.2.2. *In-Ovo* investigation of the impact of CNFs and MCNFs

2.2.2.1. Evaluation of the effect of CNFs & MCNFs treatment on the embryo

White Leghorn fertilized chicken eggs were obtained from the Arab Qatari for Poultry Production and incubated at 37ºC and 60% humidity in the MultiQuip egg incubator. All procedures were ethically approved by the Institutional Bio-safety committee of Qatar University. Four sets of experiments were conducted; 60 embryos were used for each set of experiments**.** Each embryo was treated at day 3 of incubation with 50 µg of CNFs or MCNFs dispersed in sterilized water**.**

Briefly, a small circular cut was made on the top of the eggshell and the membrane of the shell was carefully removed by adding 100 µL of PBS 1X (Sigma-Aldrich, UK). The CNFs or MCNFs treatment were added on circular coverslips (Sigma-Aldrich, UK) and were placed directly on the embryos. Embryos treated with 50 µL of sterilized water were used as control. The eggs were then sealed and incubated for a period of 5 days. Mortality incidences were recorded daily. On day 8 of incubation, embryos were sacrificed, and their brain, liver, and heart tissues were autopsied for macroscopic observation and RNA extraction for RT-PCR analysis. Four independent sets of experiments were performed to get reproducible results.

2.2.2.2. Chorioallantoic membrane (CAM) assay

Embryos at 6 days of incubation were treated with 50µg of as-prepared CNFs or MCNFs suspension which was placed on a circular glass coverslip to explore their effect on the CAM compared to controls. After 48-hours post-treatment, the effect of CNFs & MCNFs on vascular development of the CAM was evaluated daily over the

period of three days with a stereomicroscope. Two areas within the same embryo were compared; area under the coverslip (treated area) and the area surrounding the coverslip (untreated area). Images were captured and both treated and untreated areas in each embryo were quantified for branching points and total length and area of the vessels using AngioTool software version 0.6a (137). Three separate sets of experiments were conducted to obtain reproducible results. The images had the same size and magnification with unified AngioTool inputs; vessel diameter thresholds at [10,255], vessel thickness at 4 and 5, removed small particles at 200 and filled holes at 150.

2.2.2.3. RNA extraction and reverse transcription-polymerase chain reaction (RT)-PCR analysis

2.2.2.3.1. RNA Extraction:

Total RNA was purified from the brain, heart, and liver tissues of chicken embryos using the All Prep DNA/ RNA FFPE Kit (Qiagen, Valencia, CA) according to the manufacturer's protocol. Quantification of RNA concentration was carried out using the nanodrop reader (Thermo-Fisher Scientific, USA).

Briefly, 350 μL of RLT lysis buffer was added to each autopsied organ of the chicken embryo. Then, using a prop sonicator a homogenized mixed solution obtained. Afterward, the lysate was spun using centrifuge apparatus at 14,000 rpm for 3 min. The supernatant was transferred to new Eppendorf tubes (Eppendorf, Germany). Then, 750 μL of 70 % ethanol was added in each Eppendorf to precipitate the DNA out and permit the binding of RNA to the RNeasy membrane. The mixed solution was transferred in mini spin columns placed in collection tubes, then it was centrifuged at 10,000 rpm for 15 sec. After we have discarded the solution in the spin column, FRN buffer (350μL) was added, centrifuged again, and then the flow-through solution was discarded. Then,

80 μL of the mixture (10 μL of DNAse1, RNAse free + 70 μL of RDD DNA digest buffer) was added in each Eppendorf and was left for 15 min. The mixture was washed with RPE buffer twice, followed by a dry spin in a centrifuge in a new collection tube at 14,000 rpm for 15 min. Finally,30 μL of RNase free water (QIAGEN, CA, USA) was added to the spin column and centrifuged for 2 minutes. Quantification of RNA concentration was carried out using the nanodrop reader (Thermo-Fisher Scientific, USA). Only samples with 260/280 nm ratio = 2 or 2.1 (pure RNA) were considered.

2.2.2.3.2. Reverse transcription-polymerase chain reaction (RT)-PCR analysis

The Invitrogen SuperScript® III One-step RT-PCR with Platinum™ *Taq* DNA Polymerase (Invitrogen, USA) was used for both cDNA synthesis and PCR amplification following the manufacturer's protocol. The kit components were (2X Reaction Mix, SuperScript® III RT/Platinum Taq Mix, and Nuclease-free water) were left to thaw on ice)**.** In ice, A 1X RT master mix was also prepared as described in (Table 2). An appropriate amount of RT master mix (1X, Thermo-Fisher Scientific, USA) (Table 2) was placed in PCR Eppendorf (Germany).In each well of Veriti 96 well-plate thermal cycler (Applied Biosystems, Austin, TX), 11.5 μL of the prepared master mix with 1μL of extracted RNA (50 ng/μL) were added. The RT-PCR program was adjusted as follow initial denaturation for cDNA synthesis at 60 ºC for 15 min and 94 ºC for 2 min respectively, followed by a denaturation period of 40 cycles at 90 ºC for 15 sec, annealing temperature was adjusted according to the specific primer temperature stated in table 2 for 30 sec. Then, the elongation process was set at 68 ºC for 1 min followed by a final elongation process 68 ºC for 5 min. Finally, they temporarily remained in the machine at 4 ºC until they were used. On 1.5% agarose gel

(3 gm agarose+ 200ml triphosphate EDTA + 5μL cybersafe), the PCR product was run at 120 V for 1 hour.

RT-PCR amplification was performed using primer sets (Table 3) for the following genes: activating transcription factor-3 (ATF-3), forkhead box-A2 (FOXA-2), inhibin beta-A (INHIBA), microtubule-associated protein RP/EB family member-2 (MAPRE-2), receptor (TNFRSF)-interacting serine-threonine kinase-1 (RIPK-1), serpin peptidase inhibitor-4 (SERPINA-4), vascular endothelial growth factor-C (VEGF-C) and glyceraldehyde 3-phosphate dehydrogenase (GAPDH). Relative gene expression quantification was performed by analyzing the RT-PCR obtained images using the ImageJ software 1.52k (138). The intensity of the bands relative to the GAPDH bands was used to calculate a relative expression of genes in the heart, liver, and brain tissues**.**

Table 2. Master Mix for RT-PCR

Component	Volume (μL)
2X Reaction Mix	6.25
Forward Primer (10μM)	1
Reverse Primer (10μM)	1
SuperScript® III RT/Platinum Taq Mix	0.5
Nuclease-free Water	2.75
Total	11.5

Table 3. List of primers set used for RT-PCR expression

Gene	Forward Primer (5'-3')	Reverse Primer (5'-3')	Annealing Temperature (^{0}C)
FOXA-2	GACCTCTTCCCCTTCTACCG	AGGTAGCAGCCGTTCTCAAA	56
MAPRE-2	CAAAGGAGCCTTCCACAGAG	GTCACTTCTGATGGCAGCAA	56
RIPK-1	CCGTACAGAATTGCAGCAGA	TTCCATTAGCACACGAGCTG	56
INHB-A	GCCACCAAGAAACTCCATGT	GCAACGTTTTCTTGGGTGTT	46
ATF-3	AAAAGCGAAGAAGGGAAAGG	ATACAGGTGGGCCTGTGAAG	50
SERPINA-4	CCAGCAAAAGGGAAAATGAA	CACCACTGATGCCAGAGAGA	50
VEGF-C	AGGGAACACTCCAGCTCTGA	CTCCAAACTCTTTCCCCACA	50
GAPDH	CCTCTCTGGCAAAGTCCAAG	CATCTGCCCATTTGATGTTG	56

2.2.3. In-vitro evaluation of the effect of CNFs and MCNFs using embryonic fibroblast cells

2.2.3.1 Embryonic Fibroblast cells culture

Embryos of the obtained White Leghorn fertilized chicken eggs were used to prepare embryonic fibroblast cells (EFCs) at 9 days of incubation. The embryos were removed carefully from the egg under the culture hood and placed in 10 mm petri dishes. Excluding the internal organs, head, and limbs, the rest of the embryos were cut to small pieces using sterilized microsurgical equipment and incubated in 10 mm Petri dishes with 1.5ml trypsin (Invitrogen, Life Technologies) for 10 minutes. This was followed by mechanical separation using a pipette to dissolve the remaining tissue. Cells were transferred to a tube with 10ml of RPMI with 10% fetal bovine serum (FBS; Invitrogen, Life Technologies) to inactivate the trypsin and centrifuged at 1,000 rpm for 5 min. Finally, the cells pellets were resuspended in RPMI-1640 media (Thermo

Fisher Scientific, USA) supplemented with 10% fetal bovine serum (FBS; Invitrogen, Life Technologies) and 1% PenStrep antibiotic (Thermo Fisher Scientific, USA) then incubated at 37° C in a 5% CO2 atmosphere. Cells media was replaced every 48 hours.

2.2.3.2. Cell viability

In 96-well plate (Thermo Fisher Scientific, USA), 10,000 cells of EFCs/well were seeded and incubated for 24 hours to adhere. The next day, the old media was replaced with a fresh one and the cells were exposed to different concentrations of both CNFs and MCNFs (5, 15, 30, 50, 70, 100 µg/ mL). Then, after 48-hours post-treatment, the old media was discarded and replaced with fresh ones containing 2% Alamar Blue dye (Thermo Fisher Scientific, USA). The plates were incubated for 2 hours in 5% CO2 at 37° C incubator. Afterward, the Infinite m200 PRO microplate reader (TECAN, Switzerland) was used to record the fluorescence at a wavelength of 560 nm. The following formula was used to calculate % of viable cells:

$$\%\, Viability = \frac{Fluorescence\ of\ treated\ wells}{Fluorescence\ of\ control\ wells} \times 100$$

2.2.3.3. Morphological examination

Approximately 300,000 cells of EFC line model were seeded/ well in 6-wells plates (Thermo Fisher Scientific, USA) and incubated for 24-hours to adhere. Then, the next day the old media was discarded and substituted with a fresh one, and the cells were treated with CNFs or MCNFs at a concentration of 50 &100 µg/mL. The morphological characteristics of the treated and control cells were observed for 48 hours using a DMi8 inverted microscope (Leica, Germany) connected to Leica EC4 digital camera. Images were captured using Leica LAS EZ software.

2.2.3.4. Cell Cycle Analysis

Approximately, 300,000 - 400,000 EFCs/well were cultured in Low Attachment Surface Polystyrene 6-wells plates (Costar, USA) and left overnight to adhere. Twenty-four hours later, CNFs and MCNFs were added to the cells at a concentration of 70 µg/mL (that approximately correspond to the IC50 of both treatments). Then, 48-hours post-treatment, floating cells were collected and counted by Neubauer counting chamber. Afterward, ice-cold PBS was used to wash the cells and centrifuged at 4° C (200 x g for 15 minutes). The supernatant was removed and ice-cold 70% ethanol was added in a drop-wise pattern while gentle vortexing to fix the cells. The samples were preserved at - 20° C for 24-hours. On the measurement day, the samples were centrifuged at 4° C (800 x g for 15 minutes) and the supernatant solution was discarded. Then, the cells were washed twice using ice-cold PBS and each sample was stained by 500 µL of FxCycle PI/RNase staining solution® (Thermo Fisher Scientific, USA). The samples were then incubated in a shaking water bath at 37° C for 50 min in the dark. BD FACSAria III flow cytometry (BD Biosciences, USA) was used to analyze the samples and the results were processed and evaluated using the FlowJo V10 software. A number of 50,000 cells were considered statistically significant.

2.2.3.5. Western blotting analysis

Approximately, 3 million cells/dish of EFCs were seeded in 100 mm Petri dishes (Thermo Fisher Scientific, USA) and left overnight in the incubator to adhere. Then, on the next day, the cells were treated by 50 µg/mL of CNFs or MCNFs and incubated for 48-hours. Afterward, the media with floating cells was collected and centrifuged at 1000 rpm for 5 min. The supernatant was removed, and the cell palettes were resuspended using an SDS lysis buffer. Regarding, the cells attached to the Petri-

dish, 200 µL of SDS lysis buffer was added, and the cells were collected by scrapper. Samples were kept at -20° C. Pierce BCA Protein Assay Kit (Thermo Scientific, USA) used to quantify the protein according to the manufacturer protocol.

The concentration of 10 % SDS-PAGE was prepared for all experimental proteins. PageRuler™ Prestained Protein Ladder (Thermo Scientific, USA) was employed as an indicator of the size of proteins in the samples. All samples were loaded at 25 µg per 1.5 mm 15 wells comb. Using two-step gel electrophoresis, the stained samples were run (60 Volts for 15min followed by 120 Volts
for 2 hours). Then, the protein in the gels was transferred into the PVDF membrane at 100 voltage for 2 hours using wet transfer. Afterward, the PVDF membranes were blocked with 3% BSA (Thermo Fisher Scientific, USA) for 1 hour with gentle shaking and then was incubated with primary antibodies (Table 4) with gentle shaking at 4° C. On the next day, the membrane was washed three times and then secondary antibodies were added for 1-2 hours with slow shaking followed by 3 times washing. To detect proteins by chemiluminescence, Pierce™ ECL Western Blotting Substrate was used. Blots were imaged using the iBright CL1000 imaging system.

Table 4. List of the antibodies used in the western blot analysis

No.	Antibody	Source	MW of Target Protein (kDa)	Manufacturer
1	Anti-Mouse	Goat	NA	Cell Signaling Technology, Inc., USA
2	Anti-Rabbit	Goat	NA	Cell Signaling Technology, Inc., USA
3	Beta-actin	Rabbit	42	Abcam, USA
4	ERK ½	Rabbit	44, 42	Abcam, USA
5	BCL-2	Mouse	26	Abcam, USA
6	BAX	Mouse	23	Invitrogen, USA
7	JNK1,JNK2, JNK3	Rabbit	54	Abcam, USA

2.2.4. The impact of CNFs & MCNFs on the normal development of *Drosophila melanogaster*

2.2.4.1. *Drosophila* stocks:

Drosophila melanogaster was purchased from the Bloomington *Drosophila* stock center. *D. melanogaster* was maintained on regular fly food (7.5% corn syrup, 71g/L cornmeal, 9.5g/L soy flour, 16.5g/L yeast, 5.5 g/L agar, 5.5 g/L malt, 3g/ml Napagin in ethanol) (Sigma Aldrich) in a controlled environment (70% humidity, 25°C Temperature, 12-hour day/night cycle). For practicality purposes, all experiments were conducted on female flies following the international adopted protocols.

2.2.4.2. The impact of CNFs & MCNFs on the survival rate of the *Drosophila*

Survivorship assay was conducted to explore the life-extension activity accompanied by CNFs & MCNFs uptake by wild type D. Melanogaster. CNFs and MCNFs were administrated orally to wild type of female flies by mixing 50 µg/ml of each nanocarrier with Lysogeny broth medium (Sigma Aldrich). Three sets of

experiments were conducted and a total of 30 flies were assigned to each group per trial. The number of dead flies was recorded twice every day for four weeks and mean survival was calculated. The results were compared to the control of un-treated female flies.

2.2.5. Statistical Analysis:

Each experiment was repeated at least 4 times at different time intervals. For each separate experiment result, statistical analysis was applied using GraphPad prism version 8.4.3. Data are demonstrated as mean ± SEM (standard error of the mean). Differences between CNF, MCNF, and controls were evaluated based on a one-way analysis of variance (ANOVA) for repeated measured followed by Tukey's post-hoc test. IC50 values were computed using a nonlinear regression test. The survival curves of the 2 groups (treated and control) were drawn using Kaplan-Meier Estimator and a log-rank test was used to detect the significance between the two groups. The student's T-test was used to analyze blood vessel parameters of treatment groups & control (treated vs untreated area within the same embryo). The results were considered statistically significant when p-value < 0.05.

CHAPTER 3: RESULTS

3.1. CNFs and MCNFs characterization

3.1.1. Scanning Electron Microscope (SEM)

CNFs were synthesized by electrospinning apparatus followed by a carbonization process then; they were coated with a mesoporous silica layer to prepare MCNFs as explained in the methods section. Herein, (Figure2) demonstrates the morphological characteristics of the CNFs & MCNFs using SEM. SEM images display the electrospun fabricated CNFs at 3 µm magnification (Figure 2 A), 1 µm (Figure 2 B), and 500 nm (Figure 2 C). As shown, the synthesized CNFs are arbitrarily distributed and have an average diameter of approximately 300-400 nm with a length of few centimetres. Additionally, the CNFs have a smooth surface and are homogeneous without beads as displayed in (Figure 2 C). Whereas, (Figure 2 D & E) demonstrate the SEM of the CNFs coated with a mesoporous silica layer at 1 µm and (Figure 2 F) at 500 nm magnification. As expected, they have a larger diameter than the uncoated CNFs (approximately 750 nm) due to the extra added coating of silica. Besides, as shown in figure 2 D, E, and F, we were able to visualize the formation of the pores that scattered all over the CNFs surface due to the silica layer coating.

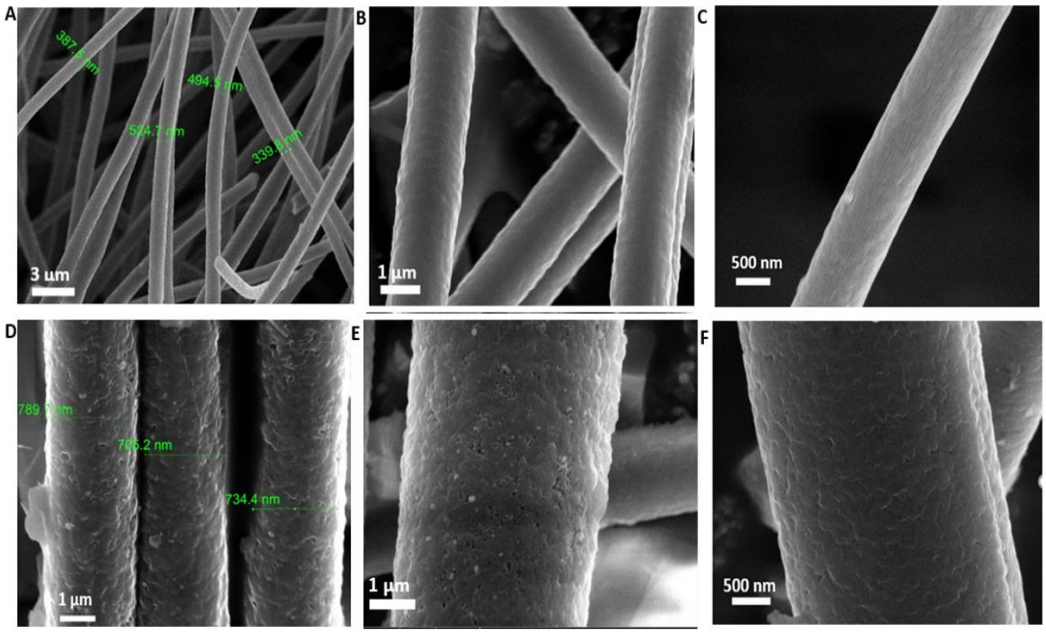

Figure 2. SEM of carbon nanofibers and Mesoporous carbon nanofibers formed from Polyacrylonitrile. (A, B, and C) SEM of CNFs at 3 µm, 1 µm & 500nm, respectively magnification; (D, E, and F) SEM of MCNFs at 1 µm, 1 µm, 500 nm, respectively magnification.

3.1.2. Mapping EDX (Energy Dispersive X-ray)

EDX and mapping were used to verify the elemental composition of synthesized CNFs and MCNFs (Figure 3). Figure 3 A shows the elemental analysis of the resultant CNFs which is constituted of approximately from 100% of carbon atoms with no noticeable impurities, thereby, confirming the efficiency of the carbonization procedure of PAN fibers to obtain high carbon yield and to eliminate all the non-carbon materials (i.e nitrogen, carbon monoxide) (139). On the other hand, Figure 3 B confirms the deposition of silica material on CNFs by revealed peaks of silicon and oxygen at 1.7 & 0.525 keV, in weight percent quantities of 0.10 &2.31 respectively. The mapping EDX (inset of Figure 3 B) depicts the uniform complete distribution of the silica material

layer on the sample.

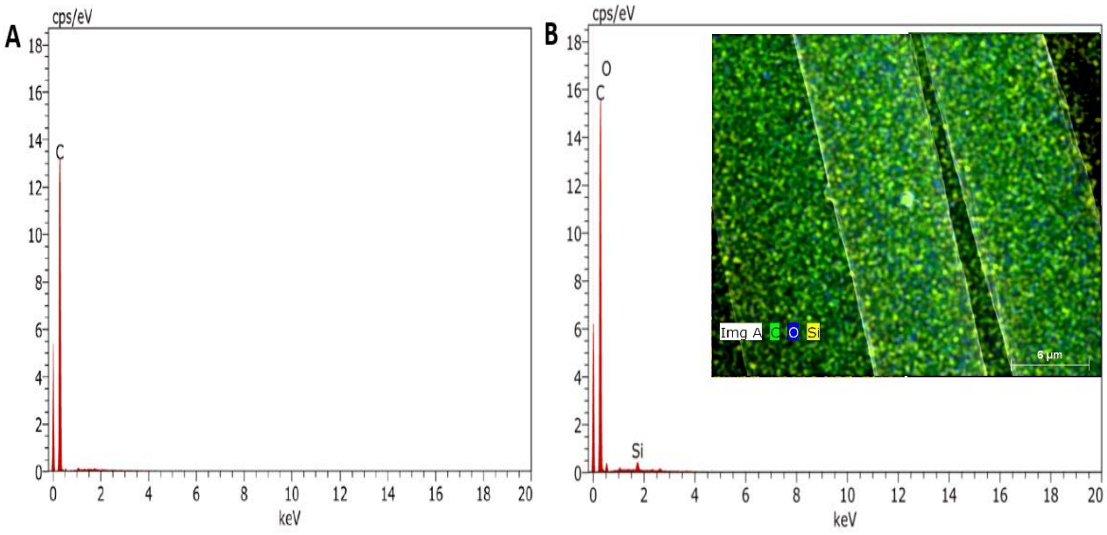

Figure 3. EDX (energy dispersive x-ray) for CNFs (Figure 3 A) and MCNFs (Figure 3 B) with inset mapping for MCNFs.

3.1.3. Transmission Electron Microscope

The morphology of MCNFs was further analyzed by a Transmission electron microscope to confirm the success of the coating process of CNFs with a mesoporous silica layer. As shown in Figure 4, we were able to visualize the mesoporous formation on the CNFs surface with an even and complete coating of CNFs. Thereby, it displays a good agreement with SEM observation.

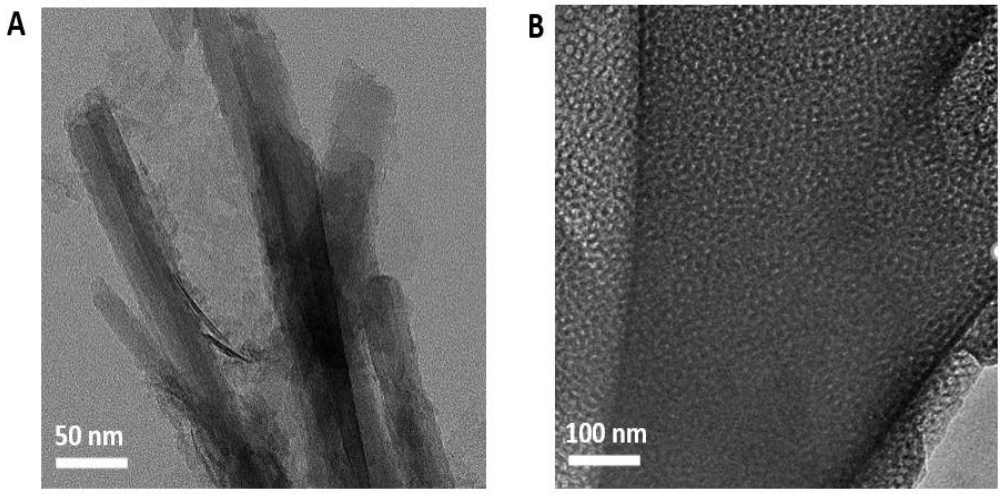

Figure 4. (A &B) Transmission electron microscope images of MCNFs.

3.1.4. X-ray Diffraction

As shown in Figure (5) is the XRD patterns of CNFs and MCNFs. The XRD pattern of the fabricated electrospun CNFs demonstrates the presence of the two characteristic broad peaks at 2 theta values of 25°and 43° of CNFs and MCNFs which indicate the (002) and (100) planes for the graphite C 2H hexagonal structure (ICCD 00-041-1487) (140). This indicates that electrospun CNFs are effectively carbonized after the calcination process at 800°C for 5 hours under nitrogen flow and showing the carbon crystalline nature with a small particle size of both CNFs and MCNFs(141). The difference in the observed intensity in the MCNFs pattern is due to the fact of the possible embedding of the carbonaceous material within the pores of the mesoporous

silica particles.

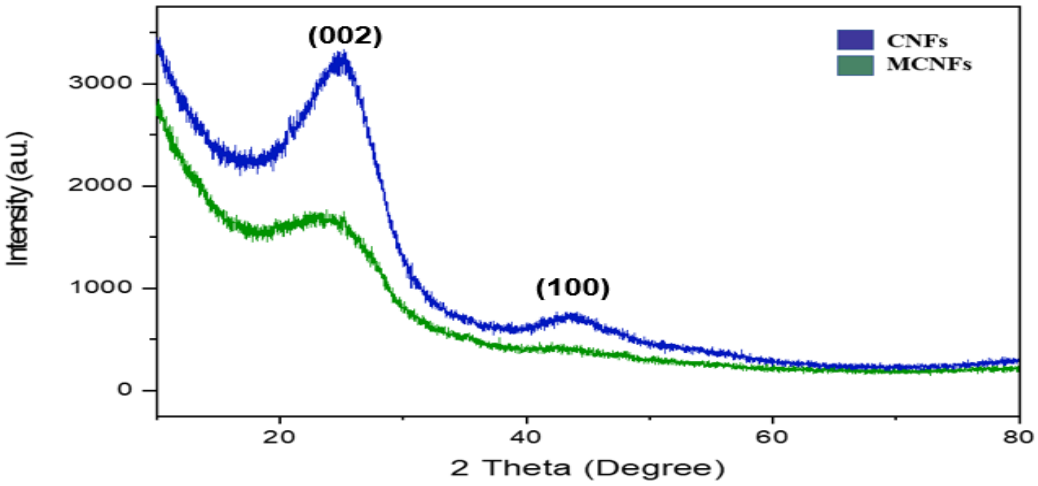

Figure 5. XRD patterns of synthesized CNFs and MCNFs.

3.1.5. Raman Spectra

Both CNFs and MCNFs were characterized via Raman spectroscopy. Raman spectroscopy is a very effective method to characterize the detailed bonding structure of carbon nanomaterials. As shown in figure 6 both CNFs samples displayed two typical distinct carbon nanomaterial peaks which are the D (assigned to the defects in carbon samples) peak at 1350 cm^{-1} and the G (assigned to ordered graphite structure) peak at ˜1575 cm^{-1}. The relative intensity ratio of D/G peaks (R = ID/IG) was calculated to measure the defects present on the carbon nanomaterials structure. The ratio values for CNFs and MCNFs were 0.97 and 0.83, respectively. It is obvious that MCNFs have higher G peak and lower R than CNFs, thus the graphitization is domain more in MCNFs (less *Sp2* bonds broken & defect) compared to CNFs.

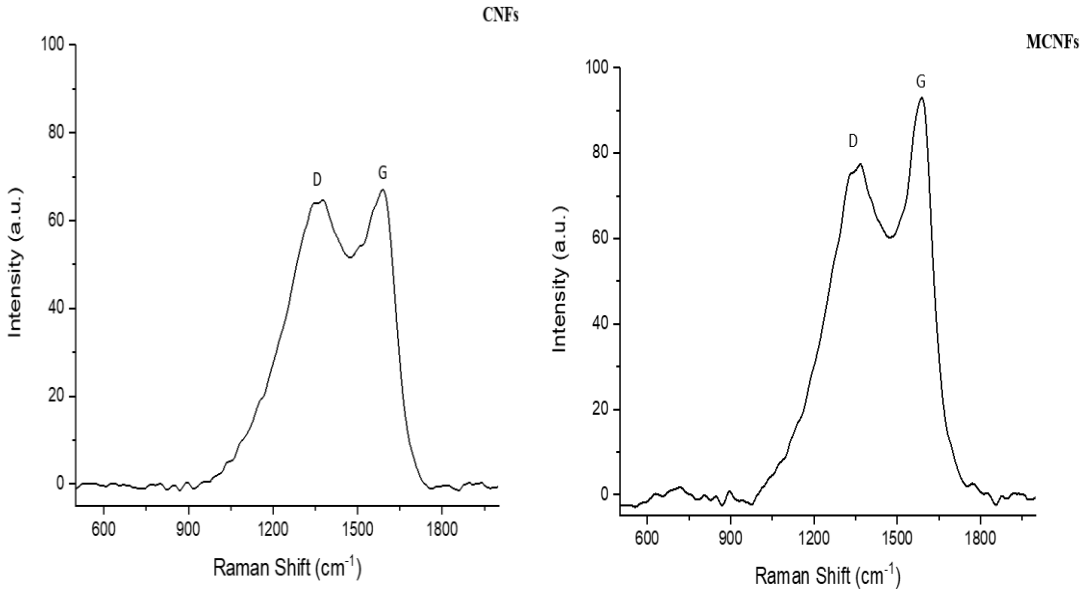

Figure 6. Raman spectra of prepared CNFs & MCNFs.

3.2. In-Vivo Toxicity Screening at The Early Stage Embryogenesis

3.2.1. Effect of CNFs and MCNFs on the normal development of the early stages of embryogenesis

To investigate the potential toxicity of CNFs and the coated CNFs with mesoporous silica layer on the early stage of embryonic development, we studied the effect of CNFs & MCNFs exposure on three-days incubated chicken embryo as described in the method section. One hundred and sixty embryos were divided equally and treated with 50 µg of the prepared CNFs or MCNFs suspension; concurrently we exposed 30 control embryos to only 50 µL of sterilized water. All embryos were monitored on daily basis for the following 5 days; it was found that 51 (~64%) of 80 embryos exposed to CNFs died compared to 35 (~44%) of 80 embryos exposed to MCNFs died 3 days post-treatment; while all the control were alive at the same period. On the 9th day of incubation 59 (~74%) of 80 CNFs-exposed embryos died compared to 42 (~53 %) of 80 MCNFs- treated embryos (P=0.0048); whereas only 2 embryos

were found dead out of 30 controls after the same duration (P< 0.0001) (Table 5). It is quite noticed that MCNFs have less mortality impact and significantly higher survival probability on the embryos compared to the CNFs (Figure 7 A). The survived embryos from the three groups were euthanized and dissected to isolate the brain, heart, and liver for further investigation. We observed that CNFs-exposed embryos considerably exhibited smaller body size and incomplete development of the brain compared to their matched controls and MCNFs treated embryos. However, MCNFs-exposed embryos did not significantly differ from the controls.

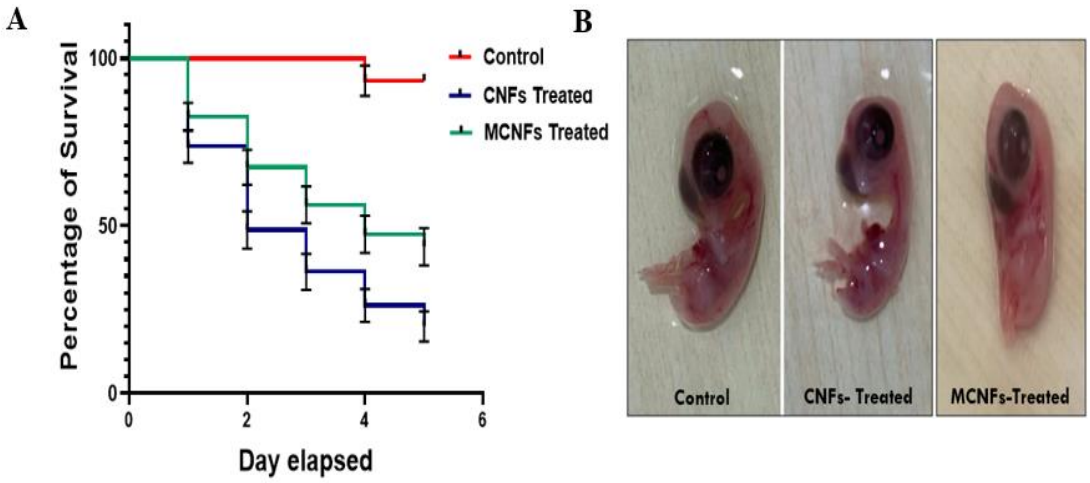

Figure 7. (A) Kaplan Mier survival curve of CNF & MCNFs-exposed embryos and their matched controls. (B) Dissected CNF and MCNFs-exposed 9 days old chicken embryo and its matched control. CNFs & MCNFs significantly reduced the survival percentage of treated embryos compared to their control (p<0.0001). Furthermore, MCNFs-exposed embryos exhibit significantly lower mortality events compared to CNFs subjected embryos (p=0.0048).

Table 5. Summary of the Outcome of CNFs & MCNFs on the embryo

Embryos groups	Sample size	The mortality rate of the embryos 6 days after exposure (%)
Controls	30	2 (3.333%)
CNFs-exposed Embryos	80	59 (~74%)
MCNFs-exposed Embryos	80	42 (~53 %)

3.2.2. The outcome of CNFs & MCNFs on the gene expression of autopsied brain, heart, and liver tissues of treated chicken embryos

We investigated the expression of 7 genes by RT-PCR methodology; namely ATF-3, FOXA-2, INHIBA, MAPRE2, RIPK-1, SERPINA-4, and VEGFC genes in the brain, heart, and liver tissues dissected from CNFs, MCNFs- exposed embryos and their matched controls. Genes were chosen regarding previous studies that evaluated the impact of single-walled CNTs (SWCNTs), and MXene (142,143) on chicken embryos; mainly due to their key regulator role in cell survival, death, proliferation, and angiogenesis. We noticed that CNFs induces significant upregulation of ATF3, FOXA2, INHIBA, MAPRE2, RIPK1 genes in the autopsied tissues compared to MCNFs and their matched control; while MCNFs causes slight non-significant upregulation of all examined genes except for MAPRE2 gene that was significantly over-expressed in brain and liver tissues ($P< 0.05$ and 0.01, respectively) (Figure 8 and 9). On the contrary, MCNFs-treated embryonic tissues exhibit more significant impact on the downregulation of both VEGF-C and SERPINA genes compared to CNFs-exposed embryonic tissues and their matched controls.

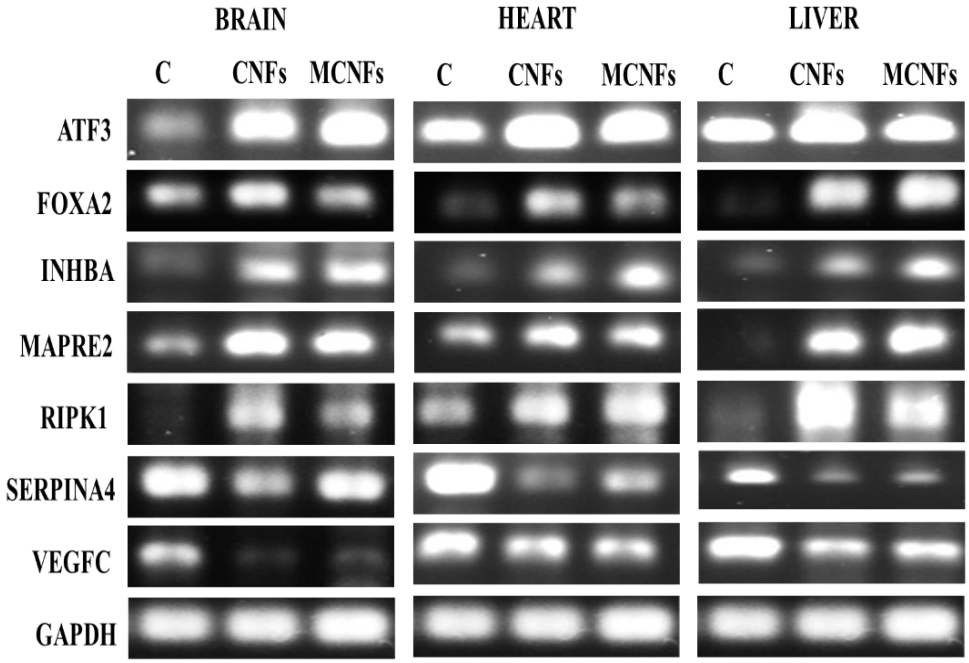

Figure 8. RT-PCR analysis of seven genes using the brain, heart, and liver tissues of chicken embryos. This analysis was performed in parallel using organ tissues obtained from both normal, CNFs and MCNFs exposed embryos. GAPDH gene was amplified from the same tissues that displayed similar loading patterns in each group.

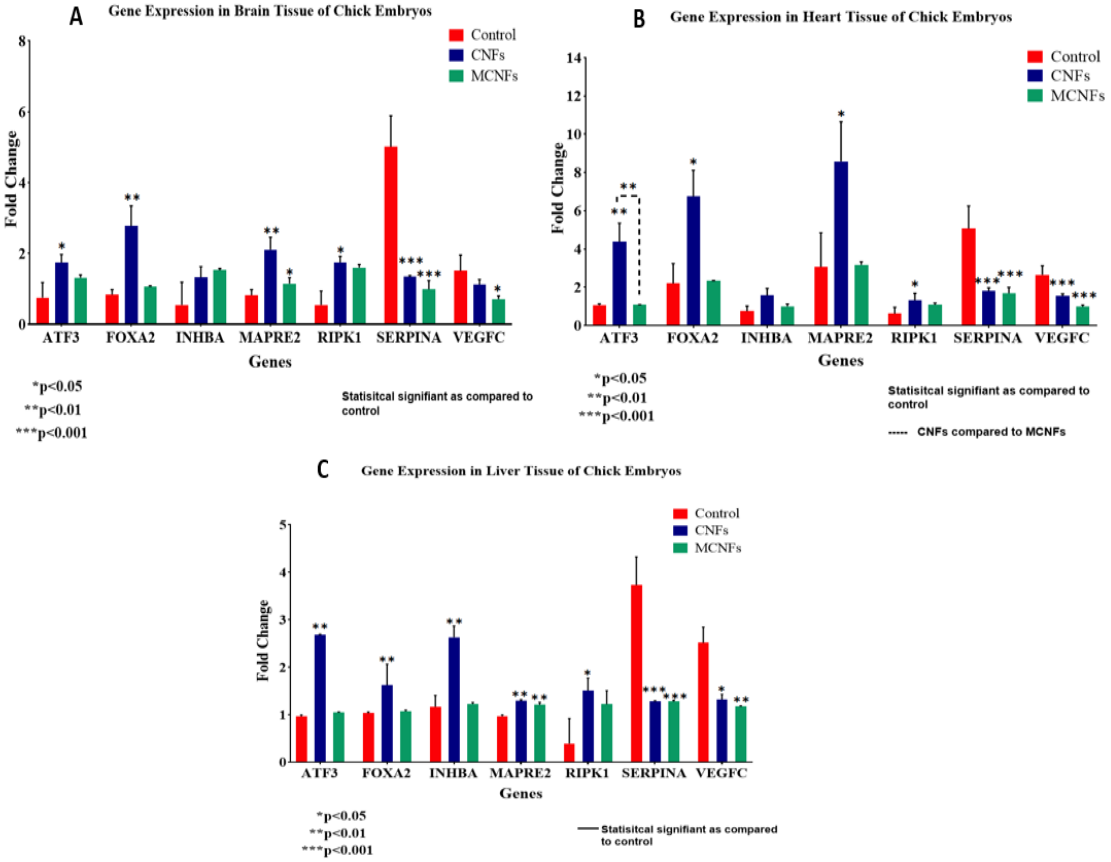

Figure 9. Quantification data of ATF3, FOXA2, INHIBA, MAPRE2, RIPK1 SERPINA4, and VEGFC genes expression of brain (A), heart (B), and liver (C) tissues of CNFs & MCNFs treated embryos and their matched controls. We noted that CNFs exposed embryos exhibit a statistically significant upregulation of ATF3, INHIBA, FOXA2, RIPK1, and MAPRE2 genes compared to their matched control and MCNFs exposed embryos. On the contrary, SERPINA4 and VEGFC are down-regulated in the tissues obtained from both MCNFs & CNFs-exposed embryos; in comparison with their matched control tissues.

3.2.3. The impact of CNFs & MCNFs on angiogenesis of the CAM model

The effect of both CNFs and MCNFs on angiogenesis was studied and compared to control using the CAM of 6 days incubated chicken embryos as illustrated in the experimental section. In agreement with survival probability outcome, MCNFs-treated embryos exhibit considerably lower death incidence than CNFs; whereas, within the first 24 post-treatment 12.5 % (5/40) of MCNFs-treated embryos died compared to CNFs-exposed embryos 27.5 % (11/40). Further mortality incidences were reported 48 hours after treatment among MCNFs-treated embryos 14.2% (5/35); while 24.1% (7/29) died of CNFs-exposure with no death incidence noticed in control. As shown in Figure (10), MCNFs found to induce a higher significant inhibition effect on blood vessel formation compared to CNFs and controls. Furthermore, we confirmed our observation by quantification of the obtained outcome for each embryo in all groups where two areas were compared and analysed outside and inside the coverslip (treated area vs untreated area) in terms of total blood vessel length, blood vessels area, and a number of junctions. Quantification analysis revealed that both CNFs and MCNFs-exposed embryos possess statistically considerably lower total blood vessels length (p<0.0001) with 21.3±3.23% and 34.9±2.08% reduction and blood vessels junction (p<0.0001) with 40.8±3.50% and 55.65±3.61% reduction, respectively as compared with their matched control, Figure 11 (A and C).

More significantly only MCNFs-treated embryos demonstrate significantly smaller blood vessels area (P<0.0001) with (27±3.35%) reduction Figure 11 (B) as compared to the controls. It is worth mentioning that MCNFs- subjected embryos exhibit lower statistical significance in terms of blood vessels area (p=0.0878) & the number of junctions (p=0.0440) as compared to CNFs-treated embryos, thus it display

notable agreement with RT-PCR analysis outcome of VEGF-C expression.

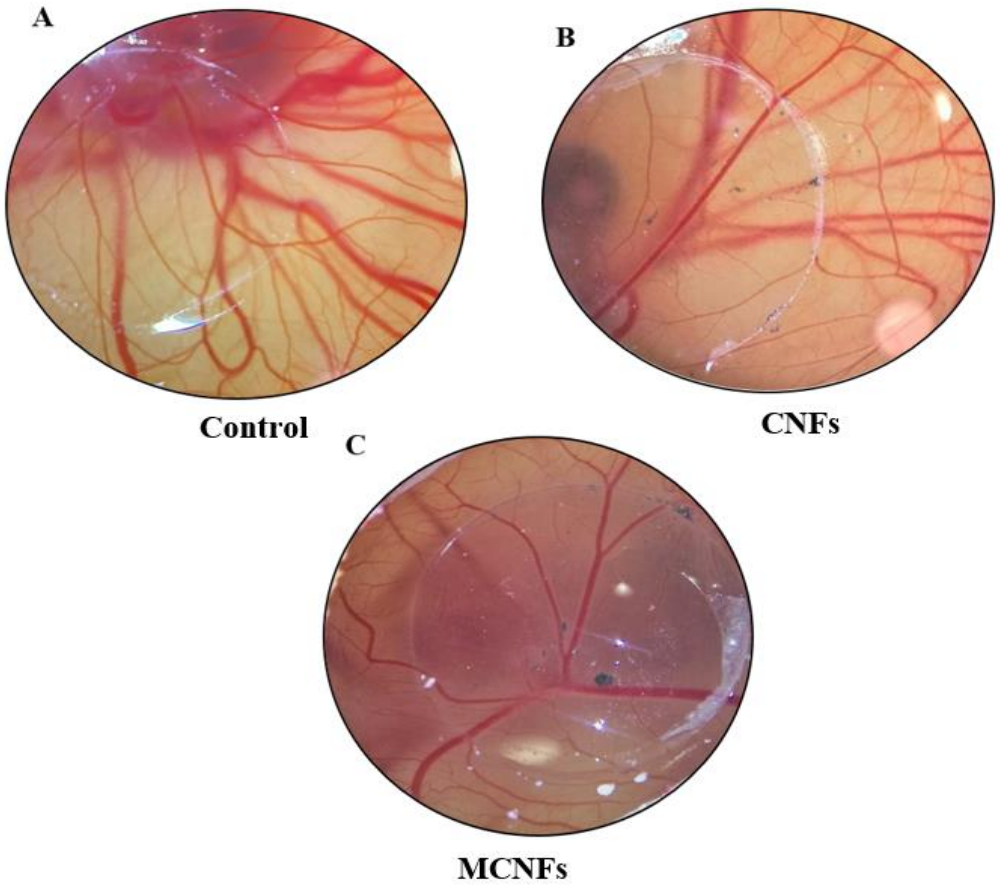

Figure 10. The impact of CNFs & MCNFs on the angiogenesis of the CAM. As compared to control (A), both CNFs (B) & MCNFs (C) prevent the angiogenesis in treated embryos compared to their control, while MCNFs was more superior in inhibition of blood vessels formation of the CAM.

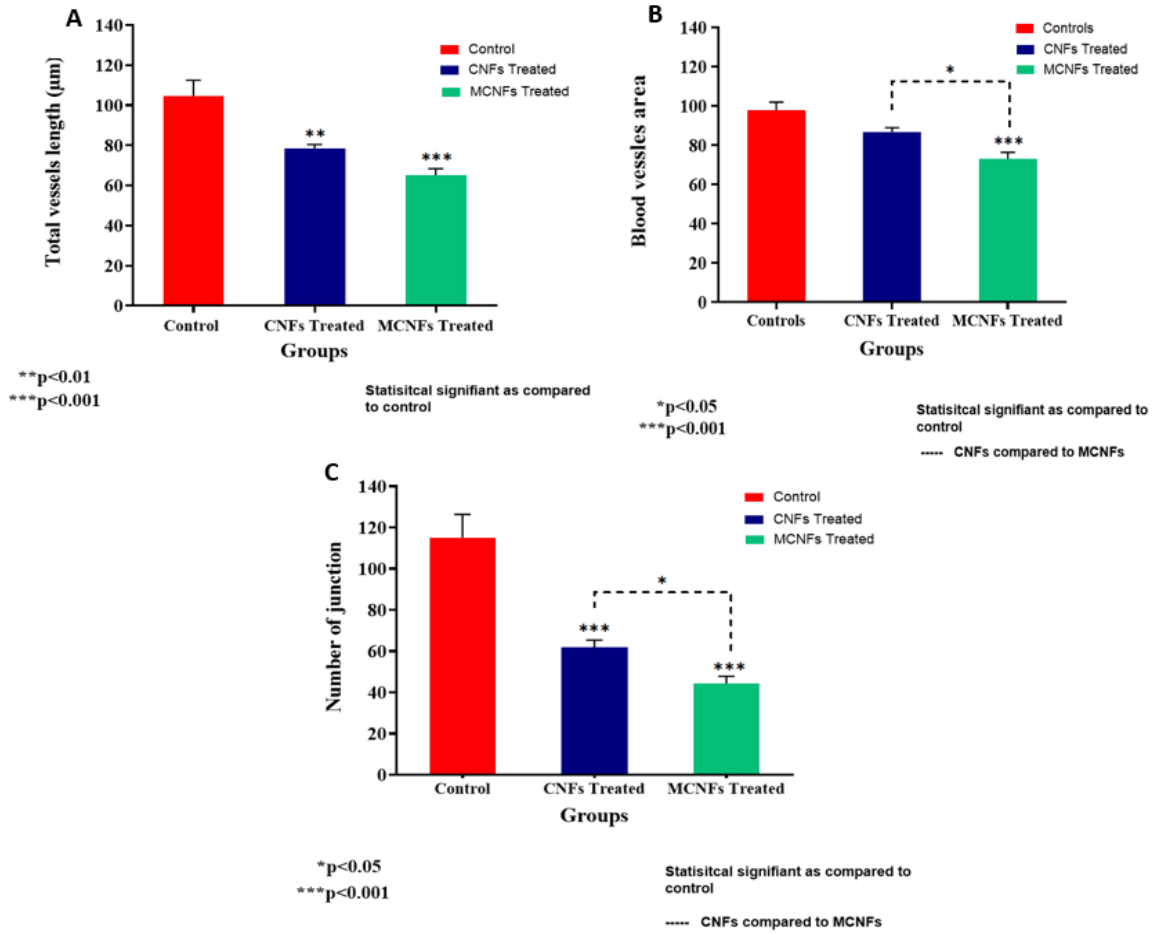

Figure 11. Quantification data of (A) Total blood vessels length of controls vs CNFs and MCNFs exposed embryos (P= 0.0012, p< 0.0001, respectively), (B) Blood vessels area of controls vs CNFs and MCNFs, only MCNFs treated embryos have statistically lower blood vessels area (P<0.0001), and (C) Number of junctions of controls vs CNFs and MCNFs treated embryos (*p*<0.0001). (**p*<0.05, ***p*<0.01, ****p*<0.001).

3.4. In-Vitro Toxicity Screening on Embryonic Fibroblast Cells

3.4.1. Effect of CNFs & MCNFs on cell proliferation

Cell Viability quantification is regarded as a valid and reliable way for investigating the cytotoxicity of different materials and drugs. Among the widely employed methods for this aim is the Alamar blue assay. Alamar blue dye (resazurin) (non-florescent, blue) contains an oxidation-reduction (REDOX) indicator that fluoresces and causes a color change (Florescent, red) due to the cell growth and can be detected using an absorbance detector. Therefore, the effect on cell viability of synthesized CNFs & MCNFs on normal embryonic fibroblast cells was compared at a concentration of (5, 15, 30, 50, 70,100) μg/mL using Alamar blue assay after 48 hours of treatment. As seen in Figure 12, the viability of the cells treated with the nanocarriers was calculated relative to the control. CNFs exposure results in a significant reduction in cell viability as compared to the control at all tested concentrations. While MCNFs treatment causes a considerable decrease in cell viability in all experimented doses except for a concentration of 5 μg/mL that did not differ significantly from the control cells. Among the CNFs & MCNFs, CNFs induced the most significant reduction in cell proliferation as compared to control ($P<0.0001$). Additionally, only at 5 μg/mL, CNFs cause a significant reduction in cell viability as compared to MCNFs ($P<0.001$). The calculated IC_{50} for CNFs and MCNFs were (70.2 μg/mL and 79.5 μg/mL, respectively).

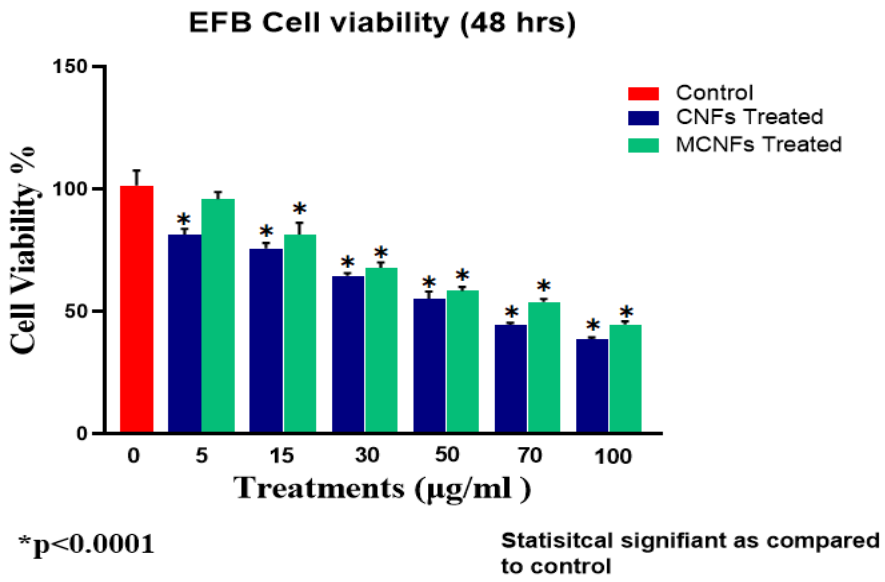

Figure 12. Effect of CNFs & MCNFs the on metabolic activity of embryonic fibroblasts cell line. The cells were treated at (5, 15,30,50,70,100) µg/mL concentration of CNFs or MCNFs and cellular proliferation was assessed after 48 hours of treatment. Values are expressed as percentage of treatment relative to the control (Mean ± SEM; n=3x3). One-way ANOVA followed by Tukey's test were used to compare the treatment groups and the data considered a statistical significance when P-value <0.05 compared to the control. (* p<0.0001)

3.4.2. Effect of CNFs & MCNFs on cell morphology

Changes in cell morphology can predict alteration in cell integrity, survival, adhesion, and genetic alterations following treatment. Therefore, a morphology study was conducted to compare the effect of CNFs & MCNFs on EFCs shapes following 48 hours of treatment. The morphology of the cells was studied following treatment of CNFs or MCNFs at a concentration of 50 µg/mL & 100 µg/mL on EFCs. Generally, as seen in Figure 13, CNFs & MCNFs at concentration 100 µg/mL induced the most

significant morphological changes. Cells exposed to CNFs at 100 µg/mL showed the highest cell death (Floating) as compared to both control and MCNFs. Furthermore, both CNFs and MCNFs exposed cells have less cell-cell adhesion comparing to control. However, the magnitude of difference observed was not that significant in CNFs & MCNFs treated cells at 50 µg/mL as compared to controls.

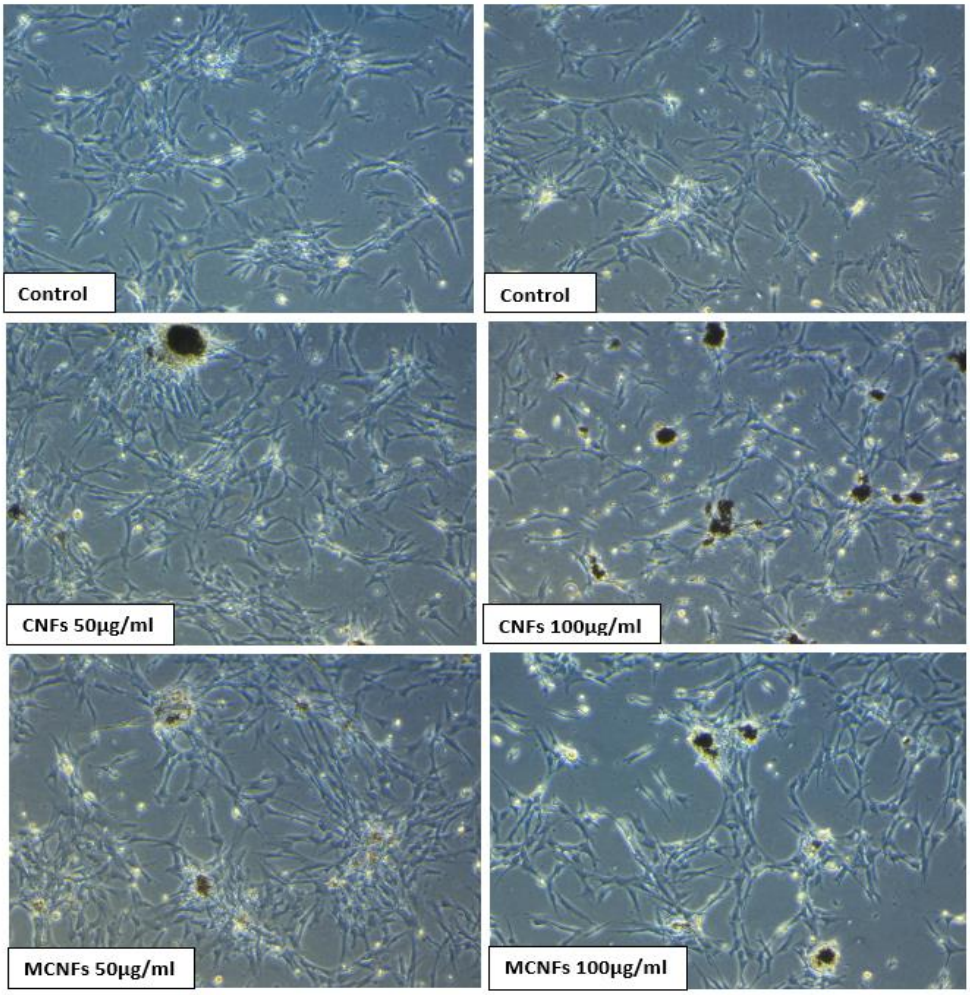

Figure 13. Effect of CNFs & MCNFs on embryonic fibroblast cells morphology at 50 µg/ml & 100 µg/ml. Images were taken at a magnification scale of 10 X and a diameter of 100 µm following 48 hours of treatment.

3.4.3. Cell cycle analysis

This experiment was performed to study the effects of CNFs & MCNFs on cell cycle progression in embryonic fibroblast cells. A flow cytometer is employed to quantify the DNA content in each phase of the cell cycle. Generally, the obtaining figures demonstrate three peaks that are assigned to the DNA present in each phase. Both treatments affect the cell cycle pattern. Our results showed that on contrary to MCNFs (10.6±0.56%, P>0.05), only CNFs induced a statistically significant cell cycle arrest in the sub G0 phase of the cell cycle in embryonic fibroblast cells (17.1± 0.70%, p<0.01) after 48 hours of exposure as compared to control (9.1±0.42%). Furthermore, a statistically significant cell cycle inhibition in the G1/G0 phase was also noticed after treatment with CNFs, while MCNFs failed to trigger a significant reduction in the G1/G0 phase (51.85± 1.62%, p<0.01and 65.45±0.91%, p>0.05) as compared to the control (68.75± 2.75%). Additionally, CNFs treatment results in significant cell cycle arrest in S phase (21.5± 1.49%, P<0.01) and G2/M phase (22.75± 1.76%, p<0.01) as compared to MCNFs and control (P>0.05),(Figure 14). Our data demonstrate that MCNFs inhibited apoptosis in normal EFCs, indicating MCNFs to have a non-toxic role

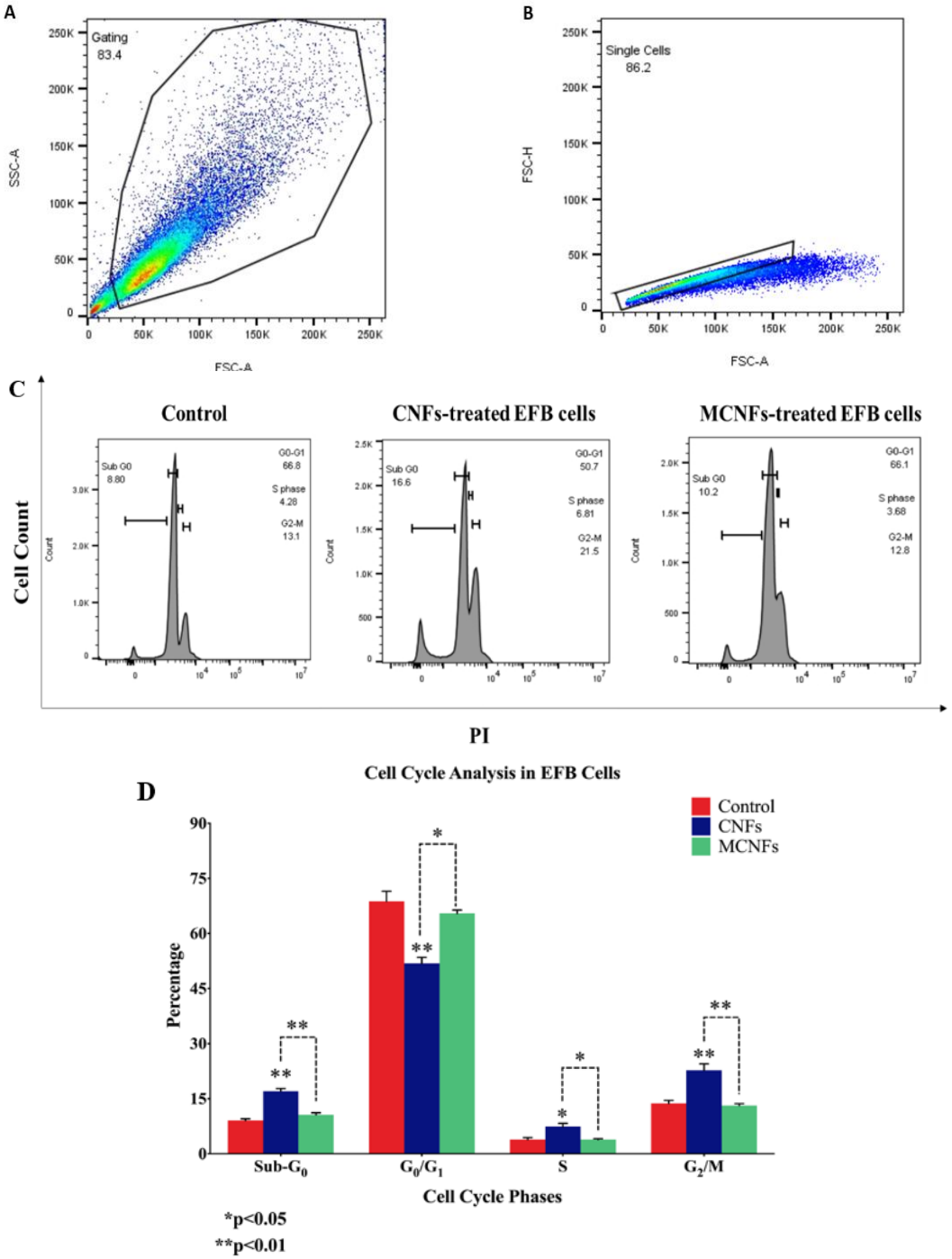
A
Gating
83.4
SSC-A
FSC-A
B
Single Cells
86.2
FSC-H
FSC-A
C
Control
CNFs-treated EFB cells
MCNFs-treated EFB cells
Cell Count
Sub G0
8.80
G0-G1
66.8
S phase
4.28
G2-M
13.1
Sub G0
16.6
G0-G1
50.7
S phase
6.81
G2-M
21.5
Sub G0
10.2
G0-G1
66.1
S phase
3.68
G2-M
12.8
PI
D
Cell Cycle Analysis in EFB Cells
Control
CNFs
MCNFs
Percentage
Sub-G0
G0/G1
S
G2/M
Cell Cycle Phases
*p<0.05
**p<0.01

Figure 14. Cell cycle analysis by flow cytometer of embryonic fibroblast cells. A) forward scatter (FSC) and side scatter (SSC) demonstrated by flow cytometry, B) single cells were gated based on their area and height on the e the forward scatter in order to exclude doublets, C) Percentage of cells in G1/G0, S, and G2/M phases, D) Cell cycle phases were quantified, and results are presented as the Mean ± SEM. Statistical analysis was performed using one-way analysis of variance (ANOVA). Tukey's post-hoc test was performed to compare treatment groups and results were considered as *statistically significant when $p<0.05$ compared to the control.

3.4.4. Effect of CNFs & MCNFs on the expression of MAPK & BCL-2 pathways on embryonic fibroblast cells

Herein, we explored the expression patterns of the main pro-apoptotic and apoptotic genes in CNFs and MCNFs-exposed embryonic fibroblast cells in comparison with their matched control (unexposed) cells. The western blot analysis showed a positive increase in BAX and downregulation of BCL-2 in the cells exposed with CNFs; meanwhile, MCNFs treated cells showed a significant decrease in BAX and up-regulation BCL-2 ratio as compared to the control (Figure 15). Thus, suggesting that MCNFs play a protective role against apoptosis in embryonic fibroblast cells by blocking the Bcl-2/Bax/ signaling pathway.

Among the crucial Mitogen-activated protein Kinase (MAPK) family members; extracellular signal-regulated kinases (ERKs) that are important for cell survival; while c-Jun N-terminal kinases (JNKs) play a crucial role in death receptor-initiated extrinsic and mitochondrial intrinsic apoptotic pathways (144). Regarding the underlying

molecular pathways of the outcome of CNFs and MCNFs on embryonic fibroblast cells, we assumed that the (MAPK) family members including ERK1/2 and (JNK) could play major roles in regulating these events; therefore, the expression patterns of ERK1/2, p-ERK1/2 and JNK1/2/3 were analyzed.

As showed in Figure 15, western blot analysis showed that total ERK 1/2 were overexpressed in CNFs and MCNFs exposed embryonic fibroblast cells; whereas both nanofibers treated embryonic fibroblast cells exhibit low activation of phospho-ERK expression as compared to control. However, regarding the ratio of p-ERK/total ERK both CNFs and MCNFs treated cells showed a statistically significant lower ratio as compared to control ($P<0.01$, $P<0.001$, respectively) (Figure 15 C). Similarly, total JNK1/2 was up regulated in CNFs treated embryonic fibroblast cells; while it was downregulated in MCNFs treated embryonic fibroblast cells.

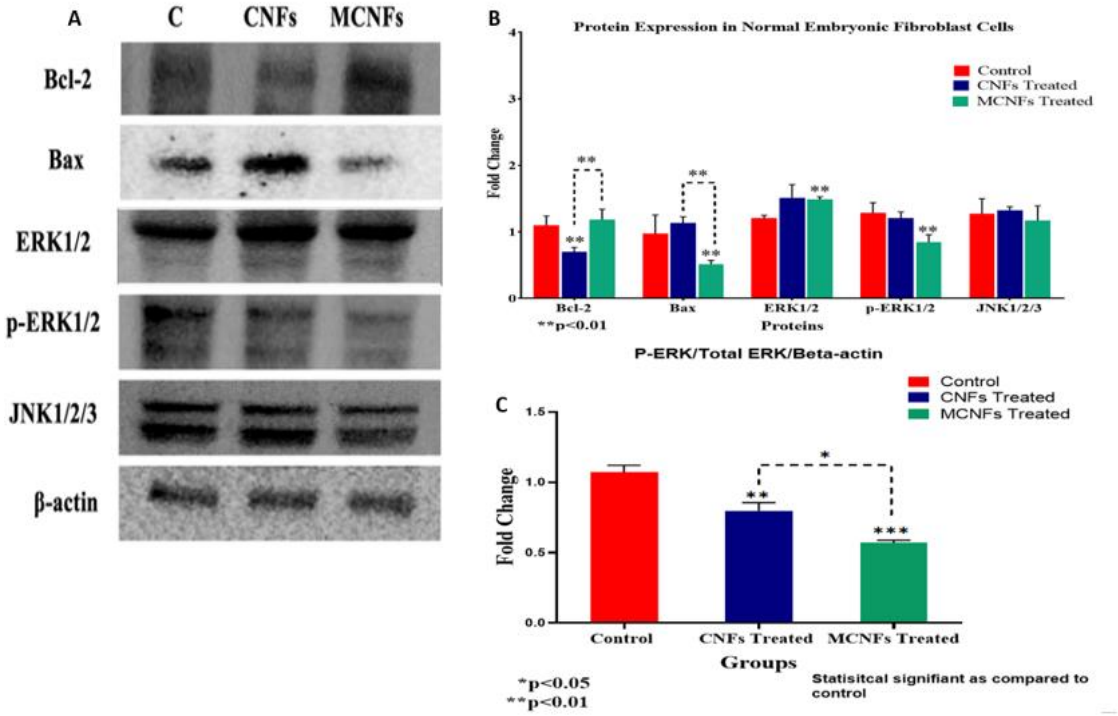

Figure 15. Protein expression and molecular mechanisms of CNFs and MCNFs inhibitory actions in normal embryonic fibroblast cells. A) Western blots representing protein expressions in cells treated with only media as control, CNFs, and MCNFs at 50 μg/mL concentrations for 48 hours. (B) Quantification of protein expression expressed as fold change of the control. (C) Ratio quantification of band densities of Phosho-ERK/Total ERK (C). Values were normalized based on the housekeeping protein β-actin. The results are presented as the Mean ± SEM.

3.5. The impact of CNFs & MCNFs on the normal development of *Drosophila melanogaster*

To confirm our toxicity data of CNFs and MCNFs on embryogenesis. We extended our investigation and studied the fabricated CNFs & MCNFs on the "*Drosophila melanogaster*" model. As described in the method section, we divided the female flies into 3 groups where they either supplemented with 50 µg/mL CNFs mixed with Lysogeny broth medium or 50 µg/mL MCNFs Lysogeny broth medium or only Lysogeny broth medium "control" as shown in Figure 16 (A and B). The number of dead flies was recorded twice every day for four weeks and mean survival was calculated. It was found that the mean lifespan of control female flies was 23.78 ±0.439 days, whereas that of CNFs and MCNFs supplemented female flies was (9.8±0.074, 15.09±0.135 days, $P<0.0001$, respectively) (Figure 16 C). Magnificently, these findings are consistent with our embryogenesis data where it is quite clear that MCNFs have less mortality effect and significantly higher survival probability on D. *melanogaster* compared to CNFs ($P<0.0001$).

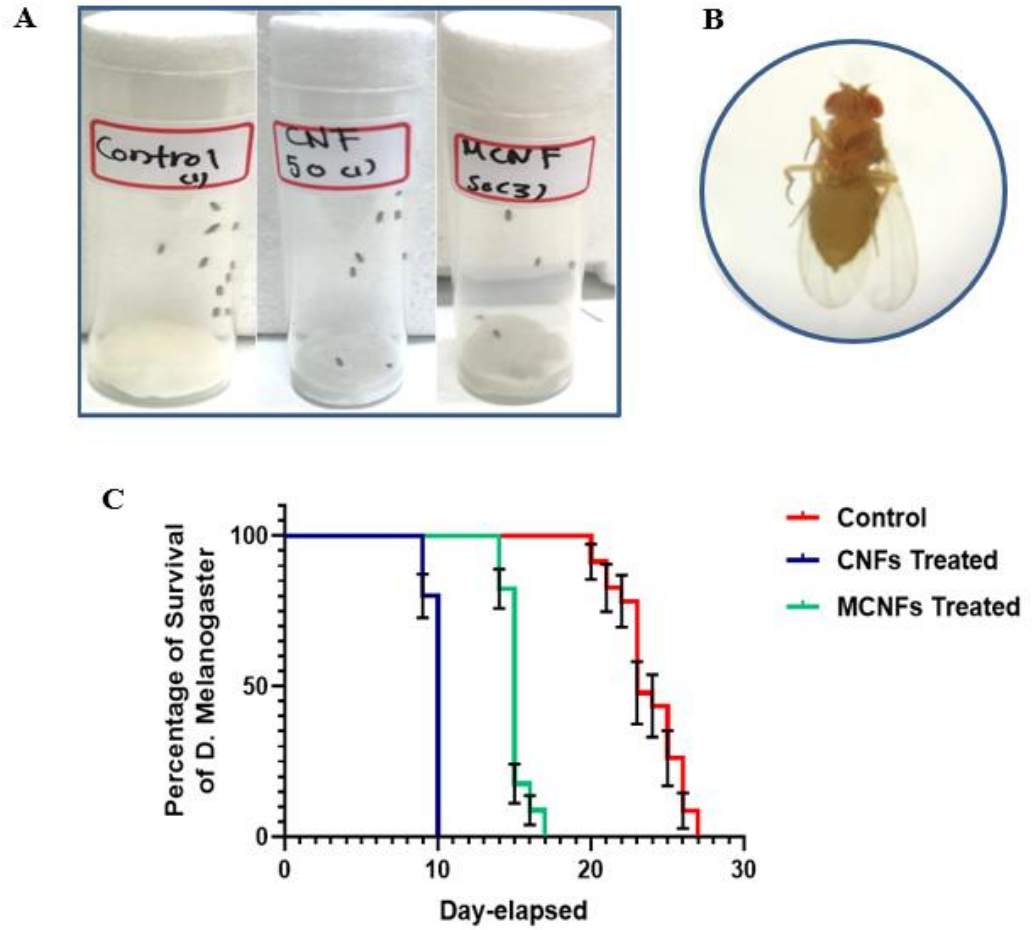

Figure 16. (A) Effect of 50 µg/mL CNFs & MCNFs oral administration on female flies' viability in *D. melanogaster* as compared to their matched control. (B) microscopic image of female fly of *D. melanogaster*. (C) Kaplan mier survival curve of CNFs and MCNFs supplemented flies. Both CNFs and MCNFs considerably reduced the survival percentage of exposed flies compared to their control (P<0.0001). Additionally, flies supplemented with MCNFs exhibit significantly reduced mortality events as compared to the CNFs administered flies (p<0.0001).

CHAPTER 4: DISCUSSION

To date, there are no general guidelines for the evaluation of CNFs potential toxicity, mainly due to the lack of sizeable reference material (145). Although, CNFs showed a great and promising contribution to the biomedical applications as in tissue engineering and drug delivery applications (22,31,33,34,63,64,146); however, reports regarding their toxicity are conflicting as well as their low dispersibility hinders their clinical application (75). Furthermore, the majority of published works have mainly focused on inhalation toxicity (76,79,145,147). In this regard, CNFs pharyngeal aspiration in mice resulted in higher events of K-ras oncogene mutation in the lungs within one-year of exposure (148). On the other hand, tissue engineering applications mediated by CNFs *in-vivo* suggest that CNFs toxicity is relatively low (69,136,149,150). Nevertheless, there is a shortage of validated data on the potential toxicity of CNFs during the early embryonic stages of vertebrate development.

On other hand, (MSNPs) were proposed as matrices for improving the apparent solubility and dissolution rate for several drugs and compounds (151,152) and are considered suitable and biocompatible for in-vivo use (153,154). However, a few *in-vitro* and *in-vivo* studies have reported the toxicity of MSNs in conjunction with human health (155–158). An *in-vivo* study by Huang et al., (2010) using xenograft mice models revealed that MSNs contribute in promoting human malignant melanoma progression (159). Conversely, several reports demonstrate that MSNs alone does not affect tumor growth using xenografted mice with human pancreatic, squamous, and breast cancer (PANC-1, KB-31, and MCF7, respectively), but chemotherapeutic loaded MSNs displayed a synergistic effect on tumor suppression(160–162). Studies using zebrafish

embryos revealed that MSNs demonstrate an efficient delivery of drug molecules without increasing the immune response as well as showed no adverse effects on their survival or development (163). Additionally, mesoporous silica in synthesized core-shell magnetic microsphere displayed overall mild acute toxicity with normal locomotion behavior, and no teratogenicity was observed in zebrafish embryos (164). Furthermore, to the best of our knowledge, the influence of MSNs on different vertebrate embryonic development has not been sufficiently studied. Thus, in this regard, we attempted to enhance the biocompatibility and safety of CNFs by coating it with a mesoporous silica layer and then, investigated their toxic effect compared to conventional CNFs on vertebrate embryonic development using the chicken embryo model.

Interestingly, unlike previous reports we obtained a homogenous suspension of both nanocarbon carriers using sterile water only (safe solvent), thus, we eliminate any possible interfering toxic effect that may arise from the solvent**.** Accordingly, we rationalized the use of the chicken embryo model would grant a crucial perception and insight on the early embryogenesis and angiogenesis (165). Consequently, for the first time, we studied the impact of CNFs and MCNFs on the expression patterns of a set of genes concerned with crucial biological events. Herein, for the first time, at studied concentration, we report that coating the CNFs with mesoporous silica layer results in less significant toxicity impact compared to the conventional CNFs in the early stage of embryogenesis and more significantly can inhibit the angiogenesis of the CAM, thus, making it an excellent nanocarrier for anticancer drug delivery applications with larger pore volume and profit for sustained release. We proved our data through exploring the effect of MCNFs treatment on crucial transcription factors and genes as compared to

CNFs as well as control, including FOXA-2 and MAPRE-2, contribute to cellular events including invasion and metastasis as well as carcinogenesis through epithelial-mesenchymal transition (166), while RIPK-1 responsible for the inflammatory response and cellular death (167), and ATF-3, plays a vital role in cellular stress response and cell proliferation (168). In addition to INHIBA that plays a crucial role in organogenesis and therefore, its upregulation leads to toxic events (169). Intriguingly, we found that embryos treated with MCNFs have slight non-significant upregulation of several key regulating genes (ATF3, FOXA2, INHIBA, RPIK1) responsible for apoptosis, survival, proliferation compared to their control; while CNFs provoke statistically significant impairment of the same genes on exposed embryos as compared to their matched controls. Though, both CNFs & MCNFs exposed embryos demonstrate considerable over-expression of MAPRE2 genes as compared to their controls. Our data were consistent with previous recent *in-vitro* studies exploring the mono-effect of mesoporous silica nanoparticles on ATF3 and FOXA2 genes (170–172). On the contrary, both MCNFs and CNFs-treated embryonic tissues exhibit significant downregulation of SERPINA4 and VEGF-C genes as compared to their control tissues. SERPINA4 gene has been previously demonstrated to be accompanied with septic shock, hypertension, cardiovascular neoplasia events in animals (173); whereas VEGF-C plays a role in blood vessel development and lymphatic system (174). Interestingly, various CNMs (fullerenes, multiwalled CNTs, and graphene) were analyzed for their anti-angiogenic effect using the CAM model; they showed larger potency in angiogenesis inhibition when linked to VEGF compared to fibroblast growth factors (FGF) in the CAM model (175). Conversely, another study (graphene and carbon nano-diamonds) proved to prevent angiogenesis *via* basal FGF downregulation; whereas they

did not influence VEGF-C expression (106). Our study shows that both CNFs & MCNFs inhibit angiogenesis in treated CAM models which could be through the downregulation of VEGF-C. In our study, MCNFs exposure led to significant impairment of blood vessels formation of the CAM 48-hours post-treatment as compared to CNFs and control. Consistently, a study by Leong et.al showed MSNs were able to abort tumor-induced angiogenesis in a size-dependent manner through reactive oxygen species production and P35 pathway activation (176).

Significantly, to confirm our embryogenesis data, we explored the impact of CNFs and MCNFs on the normal development of the *D. Melanogaster* model. Magnificently, the obtained findings were consistent with embryogenesis results, whereas MCNFs prolong the lifespan of *D. Melanogaster* by 54% comparing to CNFs supplemented flies. However, both nanocarriers demonstrate notable toxicity as compared to control. A previous report showed that chronic exposure of *D. Melanogaster* to 100 μg/ml of CNFs showed no significant developmental toxicity compared to a higher dose (1000 μg/ml); nevertheless, CNFs triggered the activation of the antioxidant defense system due to reactive oxygen species production (130). In this regard, it has been reported that the toxicity of CNFs is attributed to several factors that encompass: surface functionalization, purity, dimension, and chemical structures; as it is believed that larger forms of CNFs exhibit more cytotoxicity than its corresponding smaller and thinner forms (82).

While whole animal toxicology investigations are crucial in terms of introducing new issues of bioavailability and function. However, cellular assays in nanotoxicology studies are important to be employed to isolate and identify important biochemical toxicity pathways. Firstly, CNFs have displayed a more negative impact

on overall activity in reducing cell viability in embryonic fibroblast cells than MCNFs and CNFs.

Furthermore, our study revealed that, compared to the control and MCNFs, CNFs significantly dysregulated cell cycle of EFCs, while MCNFs did not display any significant cell cycle deregulation. This effect of MCNFs may be caused due to the early cell entry into the S phase, indicating MCNFs to be less toxic. Moreover, as compared to control and CNFs, MCNFs reduce apoptosis in the EFC line model, thus, implicating a protective role for mesoporous silica on normal cells. Therefore, we analyzed the mitochondrial apoptosis regulators of Bcl-2 family (Bcl-2 and Bax) (177). As compared to control, we found that MCNFs significantly reduce the Bax/Bcl-2 ratio in comparison to CNFs that significantly increase Bax/Bcl-2 ratio, thus, indicating that MCNFs can play a role in preventing apoptotic cell death through the intrinsic mitochondrial pathway. Consistent with our findings, Huang et al., found the MSNs cause upregulation of Bcl-2 (159). Furthermore, reduction in Bax expression indicates that MCNFs inhibit apoptosis and deregulate Bcl2/Bax-regulated cell death through JNK inactivation, as demonstrated in our study. Furthermore, inhibition in apoptotic activity in MCNFs-treated cells was confirmed by analyzing the expression of the ERK pathway. Our data are in concordance with previous studies, which revealed that loss of ERK activity is associated with downregulation of Bax along with upregulated expression of antiapoptotic members, such as Bcl-2 (178,179). We found that p-ERK1/2: total ERK1/2 was considerably downregulated in MCNFs treated cells as compared to CNFs exposed cells and control; concordant with a previous study that suggests that MSNs inhibits activation of MAPKs, further, decreasing toxicity and pro-inflammatory cytokines expression (180). However, some studies suggest that ERK1/2

activation contributes to the appropriate development of fetal lung (181). More interestingly, Studies revealed that ERK2 is essential for embryonic development and its deficiency leads to developmental defects of the placenta; while ERK1 deficient has no deterious effect mice (182,183). ERK/MAPK signaling pathway regulates several cellular processes including cell proliferation, differentiation, survival, and apoptosis (184). Previous studies indicated that inactivation of the ERK pathway causes arrest in the G_1 phase (185,186). This is concordant with our data, where CNFs and MCNFs-treated cells exhibited reduced ERK activity with a decrease in the G_0/G_1 phase of the cell cycle. Our results are in concordance with the previous studies, which showed that the inactivation of JNK and a loss of ERK expression further results in the inhibition of apoptosis. Inhibition of JNKs improves chemotherapy-induced inhibition of cancer cell growth (187–189). Intriguingly, we also noticed a slight downregulation of total JNKs in MCNFs treated cells; while, on other hand, CNFs cause upregulation of JNK1/2 as compared to control (190). Therefore, MCNFs could offer a promising nanoplatform for cancer therapy applications.

To summarize, our study reveals, for the first time, that MCNFs has significantly less toxic effect on the early onset of embryogenesis and high anti-angiogenic effect; whereas it fails to cause significant deregulation of these controller genes (ATF3, FOXA2, MAPRE-2, INHIBA, RIPK-1) as compared to CNFs, Furthermore, MCNFs showed more considerable downregulation of (SERPINA-4 and VEGFC) genes as compared to CNF. These genes are involved in the normal development of the embryo that are responsible for survival, apoptosis, cell proliferation, mitosis, organogenesis and angiogenesis. On contrary to CNFs, our findings revealed that MCNFs cause notably downregulation of active ERK/total ERK

ratio, BaX/BCL-2 ratio & total JNK, as result, it may lead to shield from cell apoptosis and toxicity.

CHAPTER 5: CONCLUSION AND FUTURE PROSPECTS

5.1. Significance of this work:

This investigation aimed to introduce a novel promising safe nanocarrier for cancer therapy by significantly decrease the carbon nanofiber (CNFs) toxicity during the embryogenesis through coating it with mesoporous silica layer (MCNFs).

Due to the increasing number of patients, especially cancer patients, the need for safe drug carriers has grown to deliver the therapeutic agents to the intended tissues only. This ensures a higher efficacy with minimal side effects. Currently, the majority of the discovered drug carrier exhibit several limitations, such as toxicity and poor biocompatibility that have a serious negative impact on the patient's health. These limitations emphasize the urgent need to discover novel safe and biocompatible drug-cargo to enhance chemotherapeutic efficiency.

CNFs showed outstanding and promising contributions in biomedical applications, including chemotherapy delivery and tissue engineering applications. However, the lack of consistent evidence about their toxicity hinders their clinical application. In this investigation, we carried out a serial of extensive comparative in-vivo and in-vitro studies to measure the toxicity of the conventional CNFs and the novel MCNFs. Consistently, the significant decrease of CNFs cytotoxicity was confirmed through our novel approach MCNFs using two different in-vivo models namely; Avian embryo and wild type of Drosophila Melanogaster (fruit flies). Furthermore, we discovered that our novel MCNFs interfere with angiogenesis which is a major source of nutrients, oxygen, and progression of cancer. Today, treatment strategies aimed toward minimizing the number of chemotherapy agents and dosing frequencies, MCNFs offer a potential promising safer nanocarrier for sustained chemotherapeutics

delivery with the advantage of the anticancer combinatory effect.

Besides chemotherapy delivery application, MCNFs is highly expected to play important role in tissue engineering application. CNFs found to improve the structural stability, mechanical strength, and conductivity of the matrix. Thus, they fasten the fractured bone's healing process (191). However, several reports demonstrate that CNFs mediated tissue engineering showed mild toxicity (69,77,192). Interestingly, MSNs have showed also beneficial characteristics for bone tissue engineering due to their low cytotoxicity, cost effectiveness, biocompatibility, and high porosity (193). Thus, MCNFs is expected to have superior the ability to deliver the small biomolecules simultaneously in sustained controlled and essential minerals lead to encourage bone cell growth without triggering immune response. Therefore, make them more appropriate, safe and biocompatible scaffolds.

5.2. Conclusion:

Implementation of carbon nanofibers (CNFs) in biomedical applications has successful outcomes, however, they are still considered as a potential hazard. we demonstrate that chicken embryo exposure to CNFs leads to significant adverse effects on the early onset of their normal development. At studied concentration, CNFs were able to cause significant mortality in embryos; meanwhile, they inhibit the angiogenesis of the CAM. Consequently, we revealed that the mechanism of CNFs toxicity is mainly due to the deregulation of key controller genes that are responsible for vital biological events during embryogenesis. However, we should highlight that various forms of CNFs with diverse purities and morphologies as well as different concentrations, exposure, dispersion, and characterization may be behind the lack of reliable CNFs toxicity studies. Interestingly, in an attempt to discover a new strategy to alleviate CNFs toxicity, for the first time, we coat the CNFs surface with a mesoporous silica layer and introduce it as a promising hit to control the CNFs toxicity. Our data shows that coating CNFs with mesoporous silica layer result in a significant reduction in the toxicity of CNFs in embryogenesis as well as the angiogenesis of the CAM. Contrary to CNFs, we revealed that MCNFs have no adverse effect on the regulation of several controller genes (ATF3, RIPIK1, FOXA2, INHIBA) that regulate the major biological events during embryogenesis. This study showed that MCNFs displayed a less significant impact on cell proliferation and morphology of embryonic fibroblast cells as compared to CNFs. Additionally, contrary to CNFs, MCNFs failed to induce a statistically significant arrest of EFCs in any cell cycle phases. While, CNFs arrested EFCs at sub-G0, S, and G2/M phases. This study reveals a substantial therapeutic potential by demonstrating cell cycle deregulation in addition to the inhibition of apoptosis by

MCNFs in normal EFCs via ERK1/2 and JNK pathways inhibition. More importantly, our data demonstrate that MCNFs exposure to EFCs protects the cells from apoptosis via the intrinsic apoptotic pathway.

Consistently to our findings, MCNFs significantly prolonged the lifespan of the *D. melanogaster* model as compared to CNFs. Taken together, our data proved that coating CNFs with a mesoporous silica layer could offer a promising solution to overcome CNFs toxicity, making them potentially more biocompatible for biomedical applications. Thus, further *in-vitro* and *in-vivo* investigations are required to clarify the effect of MCNFs at a different dose or size to determine and validate the toxicity of MCNFs exposure.

5.3. Future Prospects:

As mentioned in the previous section, several factors (size, shape, purity, and functionalization) influence the cytotoxicity of both CNFs and mesoporous silica nanoparticles. Therefore, a closer investigation of the effect of these parameters on the safety of these carriers is necessary. To this end, more investigations must be conducted using different shapes and sizes of CNFs & mesoporous materials as well as using smaller concentrations to reach optimum safety. It is worth mentioning, that mesoporous silica material has been deeply investigated as a nanocarrier, where it displayed a promising and excellent nano-cargo for targeted and sustained drug release. However, future research to delimitate the ability of the newly synthesized mesoporous silica carbon nanofibers in drug loading and release is mandatory. Finally, we do speculate that MCNFs would offer the key solution of CNFs toxicity as well as a potential of extraordinary promising nanocarrier that combines the unique advantages of CNFs and mesoporous material. This investigation opens up new avenues for promising translation of nanomedicines by achieving a balance between toxicity and biocompatibility.

REFERENCES

1. Karttunen AJ, Fässler TF, Linnolahti M, Pakkanen TA. Two-, one-, and zero-dimensional elemental nanostructures based on Ge(9)-clusters. Chemphyschem [Internet]. 2010;11(9):1944–50. Available from: http://europepmc.org/abstract/MED/20446334
2. Ruggiero A, Villa CH, Bander E, Rey DA, Bergkvist M, Batt CA, et al. Paradoxical glomerular filtration of carbon nanotubes. Proc Natl Acad Sci [Internet]. 2010;107(27):12369–74. Available from: https://www.pnas.org/content/107/27/12369
3. Lin G, Mi P, Chu C, Zhang J, Liu G. Inorganic nanocarriers overcoming multidrug resistance for cancer theranostics. Adv Sci. 2016;3(11):1600134.
4. Tiwari JN, Vij V, Kemp KC, Kim KS. Engineered carbon-nanomaterial-based electrochemical sensors for biomolecules. ACS Nano. 2016;10(1):46–80.
5. Cha C, Shin SR, Annabi N, Dokmeci MR, Khademhosseini A. Carbon-based nanomaterials: multifunctional materials for biomedical engineering. ACS Nano. 2013 Apr;7(4):2891–7.
6. Zhang D-Y, Zheng Y, Tan C-P, Sun J-H, Zhang W, Ji L-N, et al. Graphene oxide decorated with Ru (II)–polyethylene glycol complex for lysosome-targeted imaging and photodynamic/photothermal therapy. ACS Appl Mater Interfaces. 2017;9(8):6761–71.
7. Wu Y, Lin X, Zhang M. Carbon Nanotubes for Thin Film Transistor: Fabrication, Properties, and Applications. Chai Y, editor. J Nanomater [Internet]. 2013;2013:627215. Available from: https://doi.org/10.1155/2013/627215
8. Hecht DS, Hu L, Irvin G. Emerging transparent electrodes based on thin films

of carbon nanotubes, graphene, and metallic nanostructures. Adv Mater. 2011 Apr;23(13):1482–513.

9. Seo DH, Han ZJ, Kumar S, Ostrikov K (Ken). Structure-Controlled, Vertical Graphene-Based, Binder-Free Electrodes from Plasma-Reformed Butter Enhance Supercapacitor Performance. Adv Energy Mater [Internet]. 2013 Oct 1;3(10):1316–23. Available from: https://doi.org/10.1002/aenm.201300431
10. Mostofizadeh A, Li Y, Song B, Huang Y. Synthesis, properties, and applications of low-dimensional carbon-related nanomaterials. J Nanomater. 2011;2011.
11. Tuček J, Błoński P, Ugolotti J, Swain AK, Enoki T, Zbořil R. Emerging chemical strategies for imprinting magnetism in graphene and related 2D materials for spintronic and biomedical applications. Chem Soc Rev [Internet]. 2018;47(11):3899–990. Available from: http://dx.doi.org/10.1039/C7CS00288B
12. Kroto HW, Heath JR, O'Brien SC, Curl RF, Smalley RE. C60: Buckminsterfullerene. Nature. 1985;318(6042):162–3.
13. Iijima S. Helical microtubules of graphitic carbon. Nature. 1991;354(6348):56–8.
14. Novoselov KS, Geim AK, Morozov S V, Jiang D, Zhang Y, Dubonos S V, et al. Electric field effect in atomically thin carbon films. Science (80-). 2004;306(5696):666–9.
15. Pierson HO. Handbook of carbon, graphite, diamonds and fullerenes: processing, properties and applications. William Andrew; 2012.
16. Park J-M, Kim S-J, Jang J-H, Wang Z, Kim P-G, Yoon D-J, et al. Actuation of electrochemical, electro-magnetic, and electro-active actuators for carbon

nanofiber and Ni nanowire reinforced polymer composites. Compos Part B Eng [Internet]. 2008;39(7):1161–9. Available from: http://www.sciencedirect.com/science/article/pii/S1359836808000565

17. Kodama A, Ishikawa M, Lima MD. Carbon nanofiber yarn nerve scaffold. Google Patents; 2019.
18. Mordkovich V. Carbon Nanofibers: A New Ultrahigh-Strength Material for Chemical Technology. Theor Found Chem Eng. 2003 Sep 1;37:429–38.
19. Tagmatarchis N. Advances in carbon nanomaterials: Science and applications. CRC Press; 2012.
20. Bui N-N, Kim B-H, Yang KS, Dela Cruz ME, Ferraris JP. Activated carbon fibers from electrospinning of polyacrylonitrile/pitch blends. Carbon N Y [Internet]. 2009;47(10):2538–9. Available from: http://www.sciencedirect.com/science/article/pii/S000862230900308X
21. Chand S. Review Carbon fibers for composites. J Mater Sci [Internet]. 2000;35(6):1303–13. Available from: https://doi.org/10.1023/A:1004780301489
22. Saito N, Aoki K, Usui Y, Shimizu M, Hara K, Narita N, et al. Application of carbon fibers to biomaterials: a new era of nano-level control of carbon fibers after 30-years of development. Chem Soc Rev. 2011;40(7):3824–34.
23. Lu W, Zu M, Byun J-H, Kim B-S, Chou T-W. State of the art of carbon nanotube fibers: opportunities and challenges. Adv Mater. 2012 Apr;24(14):1805–33.
24. Fitzer E, Figueiredo JL, Bernardo CA, Baker RTK, Huttinger KJ. Carbon Fibers Filaments and Composites. Dordr Kluwer Acad. 1990;
25. Pei B, Wang W, Fan Y, Wang X, Watari F, Li X. Fiber-reinforced scaffolds in

soft tissue engineering. Regen Biomater. 2017;4(4):257–68.

26. Paul DR, Robeson LM. Polymer nanotechnology: Nanocomposites. Polymer (Guildf) [Internet]. 2008;49(15):3187–204. Available from: http://www.sciencedirect.com/science/article/pii/S0032386108003157

27. Baeza FJ, Galao O, Zornoza E, Garcés P. Multifunctional Cement Composites Strain and Damage Sensors Applied on Reinforced Concrete (RC) Structural Elements. Mater (Basel, Switzerland) [Internet]. 2013 Mar 6;6(3):841–55. Available from: https://pubmed.ncbi.nlm.nih.gov/28809343

28. Kenry, Lim YB, Nai MH, Cao J, Loh KP, Lim CT. Graphene oxide inhibits malaria parasite invasion and delays parasitic growth in vitro. Nanoscale. 2017 Sep;9(37):14065–73.

29. Tibbetts GG. Vapor-grown carbon fibers: Status and prospects. Carbon N Y [Internet]. 1989;27(5):745–7. Available from: http://www.sciencedirect.com/science/article/pii/000862238990208X

30. Ge M, Sattler K. Observation of fullerene cones. Chem Phys Lett [Internet]. 1994;220(3):192–6. Available from: http://www.sciencedirect.com/science/article/pii/0009261494001677

31. DE JONG KP, GEUS JW. Carbon Nanofibers: Catalytic Synthesis and Applications. Catal Rev. 2000 Nov;42(4):481–510.

32. Kim YA, Hayashi T, Endo M, Dresselhaus MS. Springer handbook of nanomaterials. Springer Berlin; 2013.

33. Feng L, Xie N, Zhong J. Carbon Nanofibers and Their Composites: A Review of Synthesizing, Properties and Applications. Mater (Basel, Switzerland) [Internet]. 2014 May 15;7(5):3919–45. Available from:

https://pubmed.ncbi.nlm.nih.gov/28788657

34. Zhang L, Aboagye A, Kelkar A, Lai C, Fong H. A review: carbon nanofibers from electrospun polyacrylonitrile and their applications. J Mater Sci. 2014;49(2):463–80.

35. Inagaki M, Yang Y, Kang F. Carbon nanofibers prepared via electrospinning. Adv Mater. 2012 May;24(19):2547–66.

36. Gopinathan J, Pillai MM, Elakkiya V, Selvakumar R, Bhattacharyya A. Carbon nanofillers incorporated electrically conducting poly ε-caprolactone nanocomposite films and their biocompatibility studies using MG-63 cell line. Polym Bull. 2016;73(4):1037–53.

37. Zagho MM, Elzatahry A. Recent Trends in Electrospinning of Polymer Nanofibers and their Applications as Templates for Metal Oxide Nanofibers Preparation. In: Electrospinning - Material, Techniques, and Biomedical Applications. InTech; 2016. p. 3–24.

38. Zagho MM, Hussein EA, Elzatahry AA. Recent Overviews in Functional Polymer Composites for Biomedical Applications. Polymers (Basel). 2018;10(7):739.

39. Hao TBT-S in IS, editor. Chapter 4 - The electrorheological materials. In: Electrorheological Fluids [Internet]. Elsevier; 2005. p. 114–51. Available from: http://www.sciencedirect.com/science/article/pii/S1383730305800195

40. Erdmann K, Ringel J, Hampel S, Wirth MP, Fuessel S. Carbon nanomaterials sensitize prostate cancer cells to docetaxel and mitomycin C via induction of apoptosis and inhibition of proliferation. Beilstein J Nanotechnol [Internet]. 2017 Jun 23;8:1307–17. Available from:

https://pubmed.ncbi.nlm.nih.gov/28690966

41. Dillip DGR, Banerjee A, V.C. A, Joo S, Min B-K, Sawant S, et al. Anchoring Mechanism of ZnO Nanoparticles on Graphitic Carbon Nanofiber Surfaces through a Modified Co-Precipitation Method to Improve Interfacial Contact and Photocatalytic Performance. Chemphyschem. 2015 Sep 4;16.

42. Wang C-J, Chen T-C, Lin J-H, Huang P-R, Tsai H-J, Chen C-S. One-step preparation of hydrophilic carbon nanofiber containing magnetic Ni nanoparticles materials and their application in drug delivery. J Colloid Interface Sci. 2015 Feb;440:179–88.

43. Arlt M, Haase D, Hampel S, Oswald S, Bachmatiuk A, Klingeler R, et al. Delivery of carboplatin by carbon-based nanocontainers mediates increased cancer cell death. Nanotechnology. 2010 Aug;21(33):335101.

44. Ringel J, Erdmann K, Hampel S, Kraemer K, Maier D, Arlt M, et al. Carbon nanofibers and carbon nanotubes sensitize prostate and bladder cancer cells to platinum-based chemotherapeutics. J Biomed Nanotechnol. 2014 Mar;10(3):463–77.

45. Dai J, Luo Y, Nie D, Jin J, Yang S, Li G, et al. pH/photothermal dual-responsive drug delivery and synergistic chemo-photothermal therapy by novel porous carbon nanofibers. Chem Eng J [Internet]. 2020;397:125402. Available from: http://www.sciencedirect.com/science/article/pii/S1385894720313942

46. Zhang DA, Rand E, Marsh M, Andrews RJ, Lee KH, Meyyappan M, et al. Carbon nanofiber electrode for neurochemical monitoring. Mol Neurobiol. 2013 Oct;48(2):380–5.

47. Guo Y, Jiang S, Grena BJB, Kimbrough IF, Thompson EG, Fink Y, et al.

Polymer Composite with Carbon Nanofibers Aligned during Thermal Drawing as a Microelectrode for Chronic Neural Interfaces. ACS Nano [Internet]. 2017 Jul 25;11(7):6574–85. Available from: https://doi.org/10.1021/acsnano.6b07550

48. Yue HY, Wu PF, Huang S, Wang ZZ, Gao X, Song SS, et al. Golf ball-like MoS(2) nanosheet arrays anchored onto carbon nanofibers for electrochemical detection of dopamine. Mikrochim Acta. 2019 May;186(6):378.

49. Kim SG, Lee JS, Jun J, Shin DH, Jang J. Ultrasensitive Bisphenol A Field-Effect Transistor Sensor Using an Aptamer-Modified Multichannel Carbon Nanofiber Transducer. ACS Appl Mater Interfaces. 2016 Mar;8(10):6602–10.

50. Cui R, Xu D, Xie X, Yi Y, Quan Y, Zhou M, et al. Phosphorus-doped helical carbon nanofibers as enhanced sensing platform for electrochemical detection of carbendazim. Food Chem. 2017 Apr;221:457–63.

51. Periyakaruppan A, Arumugam PU, Meyyappan M, Koehne JE. Detection of ricin using a carbon nanofiber based biosensor. Biosens Bioelectron [Internet]. 2011;28(1):428–33. Available from: http://www.sciencedirect.com/science/article/pii/S0956566311005094

52. Periyakaruppan A, Gandhiraman RP, Meyyappan M, Koehne JE. Label-free detection of cardiac troponin-I using carbon nanofiber based nanoelectrode arrays. Anal Chem. 2013 Apr;85(8):3858–63.

53. Gupta RK, Periyakaruppan A, Meyyappan M, Koehne JE. Label-free detection of C-reactive protein using a carbon nanofiber based biosensor. Biosens Bioelectron. 2014 Sep;59:112–9.

54. Li D, Lv P, Zhu J, Lu Y, Chen C, Zhang X, et al. NiCu Alloy Nanoparticle-Loaded Carbon Nanofibers for Phenolic Biosensor Applications. Sensors

(Basel). 2015 Nov;15(11):29419–33.

55. Rand E, Periyakaruppan A, Tanaka Z, Zhang DA, Marsh MP, Andrews RJ, et al. A carbon nanofiber based biosensor for simultaneous detection of dopamine and serotonin in the presence of ascorbic acid. Biosens Bioelectron. 2013 Apr;42:434–8.

56. Sainio S, Palomäki T, Tujunen N, Protopopova V, Koehne J, Kordas K, et al. Integrated Carbon Nanostructures for Detection of Neurotransmitters. Mol Neurobiol. 2015 Oct;52(2):859–66.

57. Eissa S, Alshehri N, Rahman AMA, Dasouki M, Abu-Salah KM, Zourob M. Electrochemical immunosensors for the detection of survival motor neuron (SMN) protein using different carbon nanomaterials-modified electrodes. Biosens Bioelectron. 2018 Mar;101:282–9.

58. Yin D, Liu J, Bo X, Guo L. Cobalt-iron selenides embedded in porous carbon nanofibers for simultaneous electrochemical detection of trace of hydroquinone, catechol and resorcinol. Anal Chim Acta. 2020 Jan;1093:35–42.

59. Motoc S, Cretu C, Costisor O, Baciu A, Manea F, Szerb EI. Cu(I) Coordination Complex Precursor for Randomized CuO(x) Microarray Loaded on Carbon Nanofiber with Excellent Electrocatalytic Performance for Electrochemical Glucose Detection. Sensors (Basel). 2019 Dec;19(24).

60. Zhang X, Liu D, Li L, You T. Direct electrochemistry of glucose oxidase on novel free-standing nitrogen-doped carbon nanospheres@carbon nanofibers composite film. Sci Rep. 2015 May;5:9885.

61. Jeong G, Oh J, Jang J. Fabrication of N-doped multidimensional carbon nanofibers for high-performance cortisol biosensors. Biosens Bioelectron. 2019

Apr;131:30–6.

62. Zhou Z, Lai C, Zhang L, Qian Y, Hou H, Reneker DH, et al. Development of carbon nanofibers from aligned electrospun polyacrylonitrile nanofiber bundles and characterization of their microstructural, electrical, and mechanical properties. Polymer (Guildf). 2009;50(13):2999–3006.

63. Tran PA, Zhang L, Webster TJ. Carbon nanofibers and carbon nanotubes in regenerative medicine. Adv Drug Deliv Rev. 2009;61(12):1097–114.

64. Elangomannan S, Louis K, Dharmaraj BM, Kandasamy VS, Soundarapandian K, Gopi D. Carbon Nanofiber/Polycaprolactone/Mineralized Hydroxyapatite Nanofibrous Scaffolds for Potential Orthopedic Applications. ACS Appl Mater Interfaces [Internet]. 2017 Feb 22;9(7):6342–55. Available from: https://doi.org/10.1021/acsami.6b13058

65. Yu Z, McKnight TE, Ericson MN, Melechko A V, Simpson ML, Morrison B 3rd. Vertically aligned carbon nanofiber as nano-neuron interface for monitoring neural function. Nanomedicine. 2012 May;8(4):419–23.

66. Mirzaei E, Ai J, Ebrahimi-Barough S, Verdi J, Ghanbari H, Faridi-Majidi R. The Differentiation of Human Endometrial Stem Cells into Neuron-Like Cells on Electrospun PAN-Derived Carbon Nanofibers with Random and Aligned Topographies. Mol Neurobiol. 2016 Sep;53(7):4798–808.

67. Malmström P-U. Intravesical therapy of superficial bladder cancer. Crit Rev Oncol Hematol. 2003 Aug;47(2):109–26.

68. Tsang M, Chun YW, Im YM, Khang D, Webster TJ. Effects of Increasing Carbon Nanofiber Density in Polyurethane Composites for Inhibiting Bladder Cancer Cell Functions. Tissue Eng Part A [Internet]. 2011 Mar 18;17(13–

14):1879–89. Available from: https://doi.org/10.1089/ten.tea.2010.0569

69. Gopinathan J, Pillai MM, Shanthakumari S, Gnanapoongothai S, Dinakar Rai BK, Santosh Sahanand K, et al. Carbon nanofiber amalgamated 3D poly-ε-caprolactone scaffold functionalized porous-nanoarchitectures for human meniscal tissue engineering: In vitro and in vivo biocompatibility studies. Nanomedicine. 2018 Oct;14(7):2247–58.

70. Meng X, Stout DA, Sun L, Beingessner RL, Fenniri H, Webster TJ. Novel injectable biomimetic hydrogels with carbon nanofibers and self assembled rosette nanotubes for myocardial applications. J Biomed Mater Res Part A. 2013;101(4):1095–102.

71. Ji H, Sun H, Qu X. Antibacterial applications of graphene-based nanomaterials: Recent achievements and challenges. Adv Drug Deliv Rev. 2016 Oct;105(Pt B):176–89.

72. Prasad K, Lekshmi GS, Ostrikov K, Lussini V, Blinco J, Mohandas M, et al. Synergic bactericidal effects of reduced graphene oxide and silver nanoparticles against Gram-positive and Gram-negative bacteria. Sci Rep. 2017 May;7(1):1591.

73. Singh S, Ashfaq M, Singh RK, Joshi HC, Srivastava A, Sharma A, et al. Preparation of surfactant-mediated silver and copper nanoparticles dispersed in hierarchical carbon micro-nanofibers for antibacterial applications. N Biotechnol. 2013 Sep;30(6):656–65.

74. Bhadauriya P, Mamtani H, Ashfaq M, Raghav A, Teotia AK, Kumar A, et al. Synthesis of Yeast-Immobilized and Copper Nanoparticle-Dispersed Carbon Nanofiber-Based Diabetic Wound Dressing Material: Simultaneous Control of

Glucose and Bacterial Infections. ACS Appl Bio Mater [Internet]. 2018 Aug 20;1(2):246–58. Available from: https://doi.org/10.1021/acsabm.8b00018

75. Oberdörster G, Castranova V, Asgharian B, Sayre P. Inhalation Exposure to Carbon Nanotubes (CNT) and Carbon Nanofibers (CNF): Methodology and Dosimetry. J Toxicol Environ Health B Crit Rev. 2015;18(3–4):121–212.

76. Donaldson K, Aitken R, Tran L, Stone V, Duffin R, Forrest G, et al. Carbon nanotubes: a review of their properties in relation to pulmonary toxicology and workplace safety. Toxicol Sci. 2006 Jul;92(1):5–22.

77. Abd El-Aziz AM, El Backly RM, Taha NA, El-Maghraby A, Kandil SH. Preparation and characterization of carbon nanofibrous/hydroxyapatite sheets for bone tissue engineering. Mater Sci Eng C Mater Biol Appl. 2017 Jul;76:1188–95.

78. Erdely A, Hulderman T, Salmen R, Liston A, Zeidler-Erdely PC, Schwegler-Berry D, et al. Cross-Talk between Lung and Systemic Circulation during Carbon Nanotube Respiratory Exposure. Potential Biomarkers. Nano Lett [Internet]. 2009 Jan 14;9(1):36–43. Available from: https://doi.org/10.1021/nl801828z

79. Kuijpers E, Pronk A, Kleemann R, Vlaanderen J, Lan Q, Rothman N, et al. Cardiovascular effects among workers exposed to multiwalled carbon nanotubes. Occup Environ Med [Internet]. 2018 May 1;75(5):351 LP – 358. Available from: http://oem.bmj.com/content/75/5/351.abstract

80. Pikula K, Chaika V, Zakharenko A, Markina Z, Vedyagin A, Kuznetsov V, et al. Comparison of the Level and Mechanisms of Toxicity of Carbon Nanotubes, Carbon Nanofibers, and Silicon Nanotubes in Bioassay with Four Marine

Microalgae. Nanomater (Basel, Switzerland) [Internet]. 2020 Mar 8;10(3):485. Available from: https://pubmed.ncbi.nlm.nih.gov/32182662

81. Magrez A, Kasas S, Salicio V, Pasquier N, Seo JW, Celio M, et al. Cellular toxicity of carbon-based nanomaterials. Nano Lett. 2006 Jun;6(6):1121–5.

82. Nagai H, Okazaki Y, Chew SH, Misawa N, Yamashita Y, Akatsuka S, et al. Diameter and rigidity of multiwalled carbon nanotubes are critical factors in mesothelial injury and carcinogenesis. Proc Natl Acad Sci U S A. 2011 Dec;108(49):E1330-8.

83. Klein KL, Melechko A V, McKnight TE, Retterer ST, Rack PD, Fowlkes JD, et al. Surface characterization and functionalization of carbon nanofibers. J Appl Phys [Internet]. 2008 Mar 15;103(6):61301. Available from: https://doi.org/10.1063/1.2840049

84. Hosamani R, Muralidhara. Acute exposure of Drosophila melanogaster to paraquat causes oxidative stress and mitochondrial dysfunction. Arch Insect Biochem Physiol. 2013;83(1):25–40.

85. Möller K, Bein T. Degradable drug carriers: vanishing mesoporous silica nanoparticles. Chem Mater. 2019;31(12):4364–78.

86. Paris JL, Colilla M, Izquierdo-Barba I, Manzano M, Vallet-Regí M. Tuning mesoporous silica dissolution in physiological environments: a review. J Mater Sci. 2017;52(15):8761–71.

87. Vallet-Regi M, Rámila A, Del Real RP, Pérez-Pariente J. A new property of MCM-41: Drug delivery system. Chem Mater. 2001;13(2):308–11.

88. Zhou Y, Quan G, Wu Q, Zhang X, Niu B, Wu B, et al. Mesoporous silica nanoparticles for drug and gene delivery. Acta Pharm Sin B. 2018 Mar;8(2):165–

77.

89. Yiu HHP, McBain SC, Lethbridge ZAD, Lees MR, Dobson J. Preparation and characterization of polyethylenimine-coated Fe3O4-MCM-48 nanocomposite particles as a novel agent for magnet-assisted transfection. J Biomed Mater Res A. 2010 Jan;92(1):386–92.

90. Kresge CT, Leonowicz ME, Roth WJ, Vartuli JC, Beck JS. Ordered mesoporous molecular sieves synthesized by a liquid-crystal template mechanism. Nature. 1992 Oct;359(6397):710–2.

91. Øye G, Sjöblom J, Stöcker M. Synthesis, characterization and potential applications of new materials in the mesoporous range. Adv Colloid Interface Sci. 2001 Jan;89–90:439–66.

92. Zhao D, Huo Q, Feng J, Chmelka BF, Stucky GD. Nonionic triblock and star diblock copolymer and oligomeric sufactant syntheses of highly ordered, hydrothermally stable, mesoporous silica structures. J Am Chem Soc. 1998 Jun;120(24):6024–36.

93. Kim I-Y, Joachim E, Choi H, Kim K. Toxicity of silica nanoparticles depends on size, dose, and cell type. Nanomedicine Nanotechnology, Biol Med. 2015;11(6):1407–16.

94. Lin W, Huang Y, Zhou X-D, Ma Y. In vitro toxicity of silica nanoparticles in human lung cancer cells. Toxicol Appl Pharmacol. 2006;217(3):252–9.

95. Tao Z, Toms BB, Goodisman J, Asefa T. Mesoporosity and functional group dependent endocytosis and cytotoxicity of silica nanomaterials. Chem Res Toxicol. 2009;22(11):1869–80.

96. Heikkilä T, Santos HA, Kumar N, Murzin DY, Salonen J, Laaksonen T, et al.

Cytotoxicity study of ordered mesoporous silica MCM-41 and SBA-15 microparticles on Caco-2 cells. Eur J Pharm Biopharm. 2010;74(3):483–94.

97. Kettiger H, Karaman D Sen, Schiesser L, Rosenholm JM, Huwyler J. Comparative safety evaluation of silica-based particles. Toxicol Vitr. 2015;30(1):355–63.

98. Lehman SE, Morris AS, Mueller PS, Salem AK, Grassian VH, Larsen SC. Silica nanoparticle-generated ROS as a predictor of cellular toxicity: mechanistic insights and safety by design. Environ Sci Nano. 2016;3(1):56–66.

99. Sweeney S, Adamcakova-Dodd A, Thorne PS, Assouline JG. Biocompatibility of Multi-Imaging Engineered Mesoporous Silica Nanoparticles: In Vitro and Adult and Fetal In Vivo Studies. J Biomed Nanotechnol [Internet]. 2017 May;13(5):544–58. Available from: https://pubmed.ncbi.nlm.nih.gov/31118876

100. Rawat N, Sandhya, Subaharan K, Eswaramoorthy M, Kaul G. Comparative in vivo toxicity assessment places multiwalled carbon nanotubes at a higher level than mesoporous silica nanoparticles. Toxicol Ind Health. 2017;33(2):182–92.

101. Rashidi H, Sottile V. The chick embryo: hatching a model for contemporary biomedical research. BioEssays [Internet]. 2009 Apr 1;31(4):459–65. Available from: https://doi.org/10.1002/bies.200800168

102. Hamburger V, Hamilton HL. A series of normal stages in the development of the chick embryo. 1951. Dev Dyn an Off Publ Am Assoc Anat. 1992 Dec;195(4):231–72.

103. McGrew MJ, Sherman A, Ellard FM, Lillico SG, Gilhooley HJ, Kingsman AJ, et al. Efficient production of germline transgenic chickens using lentiviral vectors. EMBO Rep. 2004 Jul;5(7):728–33.

104. Gagnon ZE, Patel A. Induction of metallothionein in chick embryos as a mechanism of tolerance to platinum group metal exposure. J Environ Sci Heal Part A, Toxic/hazardous Subst Environ Eng. 2007 Feb;42(3):381–7.

105. Prasek M, Sawosz E, Jaworski S, Grodzik M, Ostaszewska T, Kamaszewski M, et al. Influence of nanoparticles of platinum on chicken embryo development and brain morphology. Nanoscale Res Lett. 2013 May;8(1):251.

106. Wierzbicki M, Sawosz E, Grodzik M, Hotowy A, Prasek M, Jaworski S, et al. Carbon nanoparticles downregulate expression of basic fibroblast growth factor in the heart during embryogenesis. Int J Nanomedicine. 2013;8:3427–35.

107. Davey MG, Tickle C. The chicken as a model for embryonic development. Cytogenet Genome Res [Internet]. 2007;117(1–4):231–9. Available from: https://www.karger.com/DOI/10.1159/000103184

108. Health NI of. The public health service responds to commonly asked questions. Ilar News. 1991;33(4):68–70.

109. Silverman J, Suckow MA, Murthy S. The IACUC handbook. CRC Press; 2014.

110. Kue CS, Tan KY, LaM ML, Lee HB. Chick embryo chorioallantoic membrane (CAM): an alternative predictive model in acute toxicological studies for anti-cancer drugs. Exp Anim. 2015;14–59.

111. Barui AK, Veeriah V, Mukherjee S, Manna J, Patel AK, Patra S, et al. Zinc oxide nanoflowers make new blood vessels. Nanoscale [Internet]. 2012;4(24):7861–9. Available from: http://dx.doi.org/10.1039/C2NR32369A

112. Wierzbicki M, Sawosz E, Grodzik M, Prasek M, Jaworski S, Chwalibog A. Comparison of anti-angiogenic properties of pristine carbon nanoparticles. Nanoscale Res Lett. 2013 Apr;8(1):195.

113. Ahtzaz S, Nasir M, Shahzadi L, Amir W, Anjum A, Arshad R, et al. A study on the effect of zinc oxide and zinc peroxide nanoparticles to enhance angiogenesis-pro-angiogenic grafts for tissue regeneration applications. Mater Des [Internet]. 2017;132:409–18. Available from: http://www.sciencedirect.com/science/article/pii/S0264127517306846

114. Bikfalvi A, Klein S, Pintucci G, Rifkin DB. Biological Roles of Fibroblast Growth Factor-2*. Endocr Rev [Internet]. 1997 Feb 1;18(1):26–45. Available from: https://doi.org/10.1210/edrv.18.1.0292

115. Grodzik M, Sawosz E, Wierzbicki M, Orlowski P, Hotowy A, Niemiec T, et al. Nanoparticles of carbon allotropes inhibit glioblastoma multiforme angiogenesis in ovo. Int J Nanomedicine. 2011;6:3041–8.

116. Shinkaruk S, Bayle M, Laïn G, Déléris G. Vascular endothelial cell growth factor (VEGF), an emerging target for cancer chemotherapy. Curr Med Chem Anticancer Agents. 2003 Mar;3(2):95–117.

117. Jain RK, Duda DG, Clark JW, Loeffler JS. Lessons from phase III clinical trials on anti-VEGF therapy for cancer. Nat Clin Pract Oncol. 2006;3(1):24–40.

118. Brouillard P, Vikkula M. Genetic causes of vascular malformations. Hum Mol Genet. 2007 Oct;16 Spec No:R140-9.

119. Knudsen TB, Kleinstreuer NC. Disruption of embryonic vascular development in predictive toxicology. Birth Defects Res C Embryo Today. 2011 Dec;93(4):312–23.

120. Ugur B, Chen K, Bellen HJ. Drosophila tools and assays for the study of human diseases. Dis Model & Mech [Internet]. 2016 Mar 1;9(3):235 LP – 244. Available from:

http://dmm.biologists.org/content/9/3/235.abstract

121. Morgan TH. Sex limited inheritance in Drosophila. Science (80-). 1910;32(812):120–2.

122. Bellen HJ, Tong C, Tsuda H. 100 years of Drosophila research and its impact on vertebrate neuroscience: a history lesson for the future. Nat Rev Neurosci. 2010;11(7):514–22.

123. Siddique YH, Fatima A, Jyoti S, Naz F, Khan W, Singh BR, et al. Evaluation of the toxic potential of graphene copper nanocomposite (GCNC) in the third instar larvae of transgenic Drosophila melanogaster (hsp70-lacZ) Bg 9. PLoS One. 2013;8(12):e80944.

124. Rand MD. Drosophotoxicology: the growing potential for Drosophila in neurotoxicology. Neurotoxicol Teratol. 2010;32(1):74–83.

125. Greenspan RJ. Fly pushing: the theory and practice of Drosophila genetics. CSHL Press; 2004.

126. Pandey UB, Nichols CD. Human disease models in Drosophila melanogaster and the role of the fly in therapeutic drug discovery. Pharmacol Rev. 2011;63(2):411–36.

127. Lehmann F-O. Matching spiracle opening to metabolic need during flight in Drosophila. Science (80-). 2001;294(5548):1926–9.

128. Liu X, Vinson D, Abt D, Hurt RH, Rand DM. Differential toxicity of carbon nanomaterials in Drosophila: larval dietary uptake is benign, but adult exposure causes locomotor impairment and mortality. Environ Sci Technol. 2009;43(16):6357–63.

129. Adolfsson K, Schneider M, Hammarin G, Häcker U, Prinz CN. Ingestion of

gallium phosphide nanowires has no adverse effect on Drosophila tissue function. Nanotechnology. 2013 Jul;24(28):285101.

130. Lee S-H, Lee H-Y, Lee E-J, Khang D, Min K-J. Effects of carbon nanofiber on physiology of Drosophila. Int J Nanomedicine [Internet]. 2015 May 21;10:3687–97. Available from: https://pubmed.ncbi.nlm.nih.gov/26056448

131. Castranova V, Schulte PA, Zumwalde RD. Occupational nanosafety considerations for carbon nanotubes and carbon nanofibers. Acc Chem Res. 2013 Mar;46(3):642–9.

132. Kisin ER, Murray AR, Sargent L, Lowry D, Chirila M, Siegrist KJ, et al. Genotoxicity of carbon nanofibers: are they potentially more or less dangerous than carbon nanotubes or asbestos? Toxicol Appl Pharmacol. 2011 Apr;252(1):1–10.

133. Mittal S, Sharma PK, Tiwari R, Rayavarapu RG, Shankar J, Chauhan LKS, et al. Impaired lysosomal activity mediated autophagic flux disruption by graphite carbon nanofibers induce apoptosis in human lung epithelial cells through oxidative stress and energetic impairment. Part Fibre Toxicol [Internet]. 2017;14(1):15. Available from: https://doi.org/10.1186/s12989-017-0194-4

134. Jain S, Webster TJ, Sharma A, Basu B. Intracellular reactive oxidative stress, cell proliferation and apoptosis of Schwann cells on carbon nanofibrous substrates. Biomaterials. 2013 Jul;34(21):4891–901.

135. Naskar D, Bhattacharjee P, Ghosh AK, Mandal M, Kundu SC. Carbon Nanofiber Reinforced Nonmulberry Silk Protein Fibroin Nanobiocomposite for Tissue Engineering Applications. ACS Appl Mater Interfaces [Internet]. 2017 Jun 14;9(23):19356–70. Available from: https://doi.org/10.1021/acsami.6b04777

136. Naskar D, Ghosh AK, Mandal M, Das P, Nandi SK, Kundu SC. Dual growth factor loaded nonmulberry silk fibroin/carbon nanofiber composite 3D scaffolds for in vitro and in vivo bone regeneration. Biomaterials [Internet]. 2017;136:67–85. Available from: http://www.sciencedirect.com/science/article/pii/S0142961217303265

137. Zudaire E, Gambardella L, Kurcz C, Vermeren S. A computational tool for quantitative analysis of vascular networks. PLoS One [Internet]. 2011/11/16. 2011;6(11):e27385–e27385. Available from: https://pubmed.ncbi.nlm.nih.gov/22110636

138. Schneider CA, Rasband WS, Eliceiri KW. NIH Image to ImageJ: 25 years of image analysis. Nat Methods. 2012 Jul;9(7):671–5.

139. Rahaman MSA, Ismail AF, Mustafa A. A review of heat treatment on polyacrylonitrile fiber. Polym Degrad Stab [Internet]. 2007;92(8):1421–32. Available from: http://www.sciencedirect.com/science/article/pii/S0141391007001279

140. Babu VS, Seehra MS. Modeling of disorder and X-ray diffraction in coal-based graphitic carbons. Carbon N Y [Internet]. 1996;34(10):1259–65. Available from: http://www.sciencedirect.com/science/article/pii/0008622396000851

141. Tan J, Han Y, He L, Dong Y, Xu X, Liu D, et al. In situ nitrogen-doped mesoporous carbon nanofibers as flexible freestanding electrodes for high-performance supercapacitors. J Mater Chem A [Internet]. 2017;5(45):23620–7. Available from: http://dx.doi.org/10.1039/C7TA07024A

142. Roman D, Yasmeen A, Mireuta M, Stiharu I, Al Moustafa A-E. Significant toxic role for single-walled carbon nanotubes during normal embryogenesis.

Nanomedicine Nanotechnology, Biol Med [Internet]. 2013;9(7):945–50. Available from: http://www.sciencedirect.com/science/article/pii/S1549963413001561

143. Alhussain H, Augustine R, Hussein EA, Gupta I, Hasan A, Al Moustafa A-E, et al. MXene Nanosheets May Induce Toxic Effect on the Early Stage of Embryogenesis. J Biomed Nanotechnol. 2020;16(3):364–72.

144. Wada T, Penninger JM. Mitogen-activated protein kinases in apoptosis regulation. Oncogene [Internet]. 2004;23(16):2838–49. Available from: https://doi.org/10.1038/sj.onc.1207556

145. Fatkhutdinova LM, Khaliullin TO, Vasil'yeva OL, Zalyalov RR, Mustafin IG, Kisin ER, et al. Fibrosis biomarkers in workers exposed to MWCNTs. Toxicol Appl Pharmacol [Internet]. 2016;299:125–31. Available from: http://www.sciencedirect.com/science/article/pii/S0041008X16300382

146. Wicki A, Witzigmann D, Balasubramanian V, Huwyler J. Nanomedicine in cancer therapy: challenges, opportunities, and clinical applications. J Control release. 2015;200:138–57.

147. Guseva Canu I, Bateson TF, Bouvard V, Debia M, Dion C, Savolainen K, et al. Human exposure to carbon-based fibrous nanomaterials: A review. Int J Hyg Environ Health. 2016 Mar;219(2):166–75.

148. Shvedova AA, Yanamala N, Kisin ER, Tkach A V, Murray AR, Hubbs A, et al. Long-term effects of carbon containing engineered nanomaterials and asbestos in the lung: one year postexposure comparisons. Am J Physiol Lung Cell Mol Physiol [Internet]. 2013/11/08. 2014 Jan;306(2):L170–82. Available from: https://pubmed.ncbi.nlm.nih.gov/24213921

149. Stout DA. Recent advancements in carbon nanofiber and carbon nanotube applications in drug delivery and tissue engineering. Curr Pharm Des. 2015;21(15):2037–44.

150. Stout DA, Basu B, Webster TJ. Poly(lactic-co-glycolic acid): carbon nanofiber composites for myocardial tissue engineering applications. Acta Biomater. 2011 Aug;7(8):3101–12.

151. Wu H, Shengjian Z, Zhang J, Liu G, Shi J, Zhang L, et al. A Hollow-Core, Magnetic, and Mesoporous Double-Shell Nanostructure: In Situ Decomposition/Reduction Synthesis, Bioimaging, and Drug-Delivery Properties. Adv Funct Mater. 2011 May 24;21:1850–62.

152. Chen Y, Chen H, Guo L, He Q, Chen F, Zhou J, et al. Hollow/rattle-type mesoporous nanostructures by a structural difference-based selective etching strategy. ACS Nano. 2010 Jan;4(1):529–39.

153. Benezra M, Penate-Medina O, Zanzonico PB, Schaer D, Ow H, Burns A, et al. Multimodal silica nanoparticles are effective cancer-targeted probes in a model of human melanoma. J Clin Invest. 2011 Jul;121(7):2768–80.

154. Jaganathan H, Godin B. Biocompatibility assessment of Si-based nano- and micro-particles. Adv Drug Deliv Rev. 2012 Dec;64(15):1800–19.

155. He Q, Zhang Z, Gao F, Li Y, Shi J. In vivo biodistribution and urinary excretion of mesoporous silica nanoparticles: effects of particle size and PEGylation. Small. 2011 Jan;7(2):271–80.

156. CHEN M, HE X, SHI B, WANG K, CHEN S, ZHOU B. In vivo study of biodistribution and urinary excretion of silica nanoparticles with different size. Chinese Sci Bull. 2013;58(7):568–74.

157. He Q, Zhang Z, Gao Y, Shi J, Li Y. Intracellular localization and cytotoxicity of spherical mesoporous silica nano-and microparticles. Small. 2009;5(23):2722–9.

158. He Q, Shi J, Chen F, Zhu M, Zhang L. An anticancer drug delivery system based on surfactant-templated mesoporous silica nanoparticles. Biomaterials. 2010;31(12):3335–46.

159. Huang X, Zhuang J, Teng X, Li L, Chen D, Yan X, et al. The promotion of human malignant melanoma growth by mesoporous silica nanoparticles through decreased reactive oxygen species. Biomaterials. 2010;31(24):6142–53.

160. Lu J, Liong M, Li Z, Zink JI, Tamanoi F. Biocompatibility, biodistribution, and drug-delivery efficiency of mesoporous silica nanoparticles for cancer therapy in animals. Small. 2010 Aug;6(16):1794–805.

161. Lu J, Li Z, Zink JI, Tamanoi F. In vivo tumor suppression efficacy of mesoporous silica nanoparticles-based drug-delivery system: enhanced efficacy by folate modification. Nanomedicine. 2012 Feb;8(2):212–20.

162. Meng H, Xue M, Xia T, Ji Z, Tarn DY, Zink JI, et al. Use of size and a copolymer design feature to improve the biodistribution and the enhanced permeability and retention effect of doxorubicin-loaded mesoporous silica nanoparticles in a murine xenograft tumor model. ACS Nano. 2011 May;5(5):4131–44.

163. Sharif F, Porta F, Meijer AH, Kros A, Richardson MK. Mesoporous silica nanoparticles as a compound delivery system in zebrafish embryos. Int J Nanomedicine [Internet]. 2012/04/11. 2012;7:1875–90. Available from: https://pubmed.ncbi.nlm.nih.gov/22605936

164. Nasrallah GK, Zhang Y, Zagho MM, Ismail HM, Al-Khalaf AA, Prieto RM, et

al. A systematic investigation of the bio-toxicity of core-shell magnetic mesoporous silica microspheres using zebrafish model. Microporous Mesoporous Mater [Internet]. 2018;265:195–201. Available from: http://www.sciencedirect.com/science/article/pii/S1387181118300672

165. Shao D, Lu M-M, Zhao Y-W, Zhang F, Tan Y-F, Zheng X, et al. The shape effect of magnetic mesoporous silica nanoparticles on endocytosis, biocompatibility and biodistribution. Acta Biomater. 2017 Feb;49:531–40.

166. Kittappa R, Chang WW, Awatramani RB, McKay RDG. The foxa2 gene controls the birth and spontaneous degeneration of dopamine neurons in old age. PLoS Biol. 2007 Dec;5(12):e325–e325.

167. Dondelinger Y, Delanghe T, Rojas-Rivera D, Priem D, Delvaeye T, Bruggeman I, et al. MK2 phosphorylation of RIPK1 regulates TNF-mediated cell death. Nat Cell Biol. 2017;19(10):1237–47.

168. Song Q, Chen Q, Wang Q, Yang L, Lv D, Jin G, et al. ATF-3/miR-590/GOLPH3 signaling pathway regulates proliferation of breast cancer. BMC Cancer. 2018;18(1):255.

169. Gurdon JB, Harger P, Mitchell A, Lemaire P. Activin signalling and response to a morphogen gradient. Nature. 1994 Oct;371(6497):487–92.

170. Wang M, Yang X, Zhang P, Cai L, Yang X, Chen Y, et al. Sustained Delivery Growth Factors with Polyethyleneimine-Modified Nanoparticles Promote Embryonic Stem Cells Differentiation and Liver Regeneration. Adv Sci [Internet]. 2016 Aug 1;3(8):1500393. Available from: https://doi.org/10.1002/advs.201500393

171. Wang M, Yu J, Cai L, Yang X. Direct reprogramming of mouse fibroblasts into

hepatocyte-like cells by polyethyleneimine-modified nanoparticles through epigenetic activation of hepatic transcription factors. Mater Today Chem [Internet]. 2020;17:100281. Available from: http://www.sciencedirect.com/science/article/pii/S2468519420300410

172. Meka AK, Jenkins LJ, Dàvalos-Salas M, Pujara N, Wong KY, Kumeria T, et al. Enhanced Solubility, Permeability and Anticancer Activity of Vorinostat Using Tailored Mesoporous Silica Nanoparticles. Pharmaceutics. 2018 Dec;10(4).

173. Chao J, Bledsoe G, Chao L. Protective Role of Kallistatin in Vascular and Organ Injury. Hypertens (Dallas, Tex 1979) [Internet]. 2016/07/18. 2016 Sep;68(3):533–41. Available from: https://pubmed.ncbi.nlm.nih.gov/27432868

174. Küchler AM, Gjini E, Peterson-Maduro J, Cancilla B, Wolburg H, Schulte-Merker S. Development of the Zebrafish Lymphatic System Requires Vegfc Signaling. Curr Biol [Internet]. 2006;16(12):1244–8. Available from: http://www.sciencedirect.com/science/article/pii/S0960982206016095

175. Murugesan S, Mousa SA, O'Connor LJ, Lincoln DW, Linhardt RJ. Carbon inhibits vascular endothelial growth factor- and fibroblast growth factor-promoted angiogenesis. FEBS Lett [Internet]. 2007 Mar 20;581(6):1157–60. Available from: https://doi.org/10.1016/j.febslet.2007.02.022

176. Setyawati MI, Leong DT. Mesoporous silica nanoparticles as an antitumoral-angiogenesis strategy. ACS Appl Mater Interfaces. 2017;9(8):6690–703.

177. Lei K, Nimnual A, Zong W-X, Kennedy NJ, Flavell RA, Thompson CB, et al. The Bax subfamily of Bcl2-related proteins is essential for apoptotic signal transduction by c-Jun NH(2)-terminal kinase. Mol Cell Biol [Internet]. 2002 Jul;22(13):4929–42. Available from:

https://pubmed.ncbi.nlm.nih.gov/12052897

178. Liu J, Mao W, Ding B, Liang C. ERKs/p53 signal transduction pathway is involved in doxorubicin-induced apoptosis in H9c2 cells and cardiomyocytes. Am J Physiol Circ Physiol. 2008;295(5):H1956–65.

179. Cagnol S, Chambard J. ERK and cell death: mechanisms of ERK-induced cell death–apoptosis, autophagy and senescence. FEBS J. 2010;277(1):2–21.

180. Lee S, Yun H-S, Kim S-H. The comparative effects of mesoporous silica nanoparticles and colloidal silica on inflammation and apoptosis. Biomaterials. 2011;32(35):9434–43.

181. Nishimoto S, Nishida E. MAPK signalling: ERK5 versus ERK1/2. EMBO Rep. 2006 Aug;7(8):782–6.

182. Giroux S, Tremblay M, Bernard D, Cardin-Girard JF, Aubry S, Larouche L, et al. Embryonic death of Mek1-deficient mice reveals a role for this kinase in angiogenesis in the labyrinthine region of the placenta. Curr Biol. 1999 Apr;9(7):369–72.

183. Pagès G, Guérin S, Grall D, Bonino F, Smith A, Anjuere F, et al. Defective thymocyte maturation in p44 MAP kinase (Erk 1) knockout mice. Science. 1999 Nov;286(5443):1374–7.

184. Torii S, Yamamoto T, Tsuchiya Y, Nishida E. ERK MAP kinase in G cell cycle progression and cancer. Cancer Sci. 2006 Aug;97(8):697–702.

185. Roovers K, Assoian RK. Integrating the MAP kinase signal into the G1 phase cell cycle machinery. Bioessays. 2000;22(9):818–26.

186. Zheng X, Ou Y, Shu M, Wang Y, Zhou Y, Su X, et al. Cholera toxin, a typical protein kinase A activator, induces G1 phase growth arrest in human bladder

transitional cell carcinoma cells via inhibiting the c-Raf/MEK/ERK signaling pathway. Mol Med Rep. 2014;9(5):1773–9.

187. Wu Q, Wu W, Jacevic V, Franca TCC, Wang X, Kuca K. Selective inhibitors for JNK signalling: a potential targeted therapy in cancer. J Enzyme Inhib Med Chem [Internet]. 2020;35(1):574–83. Available from: https://doi.org/10.1080/14756366.2020.1720013

188. Huang H-L, Chao M-W, Li Y-C, Chang L-H, Chen C-H, Chen M-C, et al. MPT0G066, a novel anti-mitotic drug, induces JNK-independent mitotic arrest, JNK-mediated apoptosis and potentiates antineoplastic effect of cisplatin in ovarian cancer. Sci Rep. 2016;6(1):1–11.

189. Bubici C, Papa S. JNK signalling in cancer: in need of new, smarter therapeutic targets. Br J Pharmacol. 2014;171(1):24–37.

190. Tournier C, Hess P, Yang DD, Xu J, Turner TK, Nimnual A, et al. Requirement of JNK for stress-induced activation of the cytochrome c-mediated death pathway. Science. 2000 May;288(5467):870–4.

191. Shabafrooz V, Mozafari M, Vashaee D, Tayebi L. Electrospun nanofibers: from filtration membranes to highly specialized tissue engineering scaffolds. J Nanosci Nanotechnol. 2014 Jan;14(1):522–34.

192. Zhang H, Yu M, Xie L, Jin L, Yu Z. Carbon-Nanofibers-Based Micro-/Nanodevices for Neural-Electrical and Neural-Chemical Interfaces. Lin T, editor. J Nanomater [Internet]. 2012;2012:280902. Available from: https://doi.org/10.1155/2012/280902

193. Eivazzadeh-Keihan R, Chenab KK, Taheri-Ledari R, Mosafer J, Hashemi SM, Mokhtarzadeh A, et al. Recent advances in the application of mesoporous silica-

based nanomaterials for bone tissue engineering. Mater Sci Eng C [Internet]. 2020;107:110267. Available from: http://www.sciencedirect.com/science/article/pii/S0928493119325032